4.3. The Düzce Fault: coseismic and short/long-term geomorphic expression

4.3.1. The1999 coseismic fault trace (CFT)

Even though the kinematics of the Düzce fault is dominantly strike-slip, field observations show the presence of widespread vertical motion. The slip distribution curve (fig. 4.3.1), built by integrating the data collected by Akyuz et al. [2000 and 2002] with more than 350 new measures (see Appendix I-II), exhibit a large along strike variability, with 5.0 m maximum and 2.4 m average dextral offsets, and 2.5 m maximum vertical offset. Because the coseismic strike-slip is directly related to the movement along the seismogenic fault, the lower measured values, that cause such a great variability of the slip distribution, can be seen as due to mechanical problem (*i.e.*, bad connection between the rupture of the fault and the surface ruptures). If this is correct, the interpolation of the maximum values (fig. 4.3.1) describes the coseismic movement at the surface. The coseismic dip-slip distribution is more complex, since many gravity effects and local transtensional or transpressional components can be involved. In general the geodetic coseismic measures highlighted by GPS and InSAR data (maximum offsets: 3.5 m dextral; 1.5 m vertical) [Bürgmann et al., 2002; Çakir et al., 2003a] result to be lower than those observed in the field.

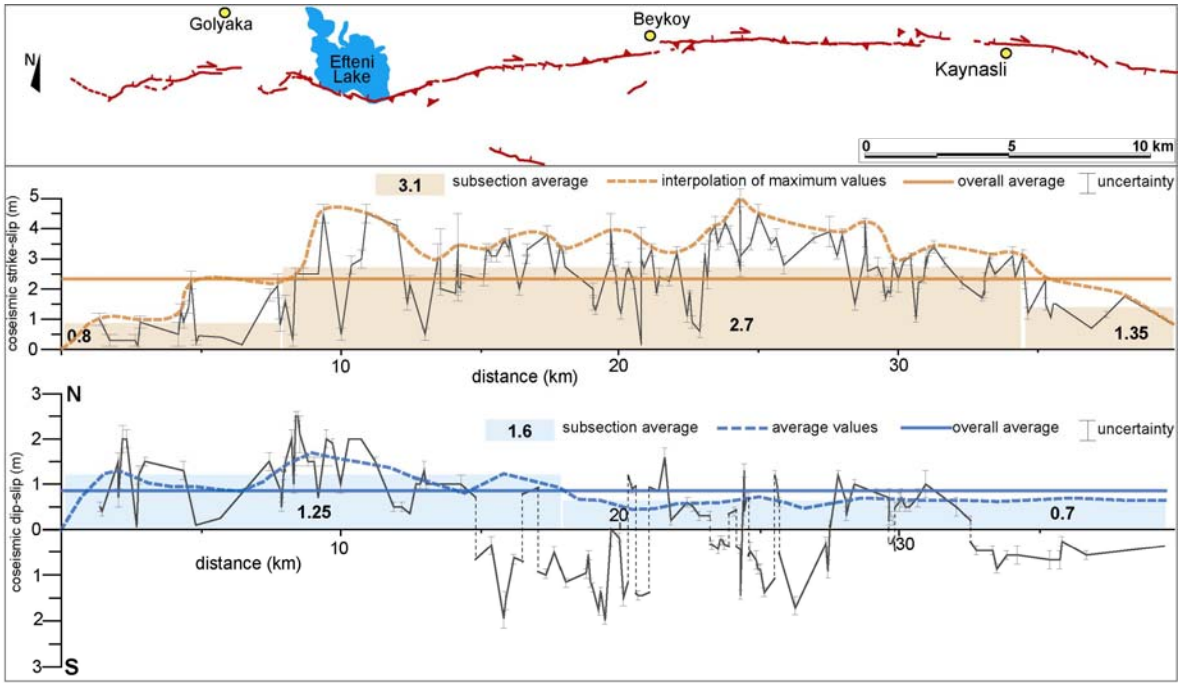

Figure 4.3.1. Horizontal and vertical slip distribution along the CFT in the study area. The relative dip-slip direction of movement is provided separate for North (N) and South (S) side down. Uncertainties have been evaluated by measuring minimum and maximum of the displacement and their range depends on the type of piercing point used.

The main characteristics of the slip distribution are: (1) the dextral coseismic offset of the CFT has a bow-shape, with slip tapering off at both ends (west of Efteni Lake and east of Kaynasli) whereas the central part has a constant and larger mean value of 2.7 m; (2) the vertical component of the western section of the CFT is higher than that of the eastern section and increases considerably the rake of the rupture toward transtensional values (fig. 4.3.2); (3) the overall westernmost section produced uplift of the range front to the south, with respect to the plain to the north; (4), frequent changes of dip-slip direction in the central part of the CFT; (5) the eastern part of the CFT produced relative subsidence of the northern block west of the Kaynasli basin and of the southern block east of it (fig. 4.3.1).

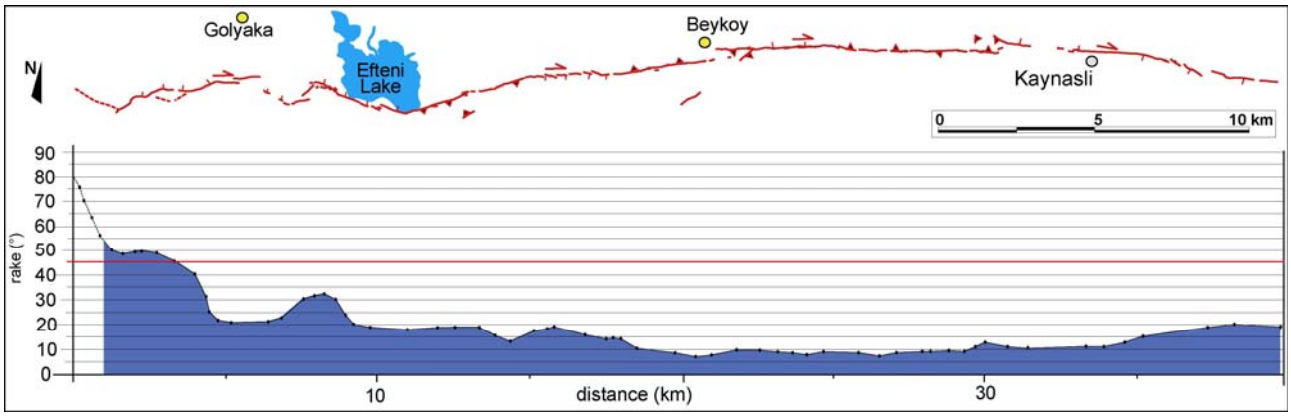

Figure 4.3.2. Synthetic rake distribution of the 1999 ruptures calculated from the ratio between dip-slip and strike-slip component (0° indicates pure strike-slip, 90° indicates pure dip-slip).

The CFT does not continuously run at the mountain-piedmont junction, but crosses the mountain front and affects both basin infill deposits and bedrock. As a whole, the CFT can be divided into two main sections, joining close to the village of Cakirhaciibrahim (fig. 4.3.3). With respect to the mean E-W trend of the Düzce fault, the western section presents sharp changes in the strike direction, producing a saw-toothed trajectory, consisting of WSW-ENE and WNW-ESE trending elements. Moving to the Cakirhaciibrahim area, the saw-toothed setting leaves space to a simpler, E-W trending trace. Conversely, the eastern CFT shows a mainly rectilinear E-W trending

trajectory, and contains two small, 1km-wide, left-steps, near Beykoy and west of Kaynasli (fig. 4.3.3).

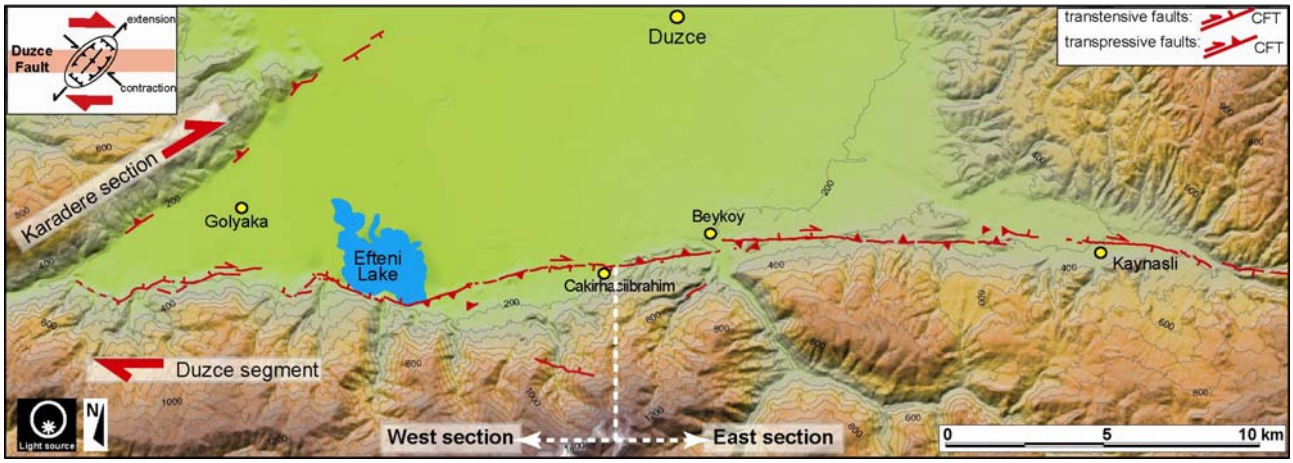

Figure 4.3.3. Sketch of the west and east sections of the 1999 ruptures (CFT). Shaded relief based on digital elevation model (DEM, interpolated from 10 m contours and auxiliary 5 m contours of 1:25.000 scale topographic maps). Contour interval 100 m. Inset shows the strain ellipse related to the shear couple of the Düzce master fault (red arrows), trend of structures related to its extensional and compressional components (black arrows) are reported.

Rose diagrams of the 1999 ruptures have been plotted to compare the coseismic structures at the different scales of observation (fig. 4.3.4). Each plot refers to fault subsections selected on the basis of their average trend and is composed by meter-scale ruptures (MSR), SDZ's and PDZ's trends. Along the east section, subsections from 5 to 8 show a general agreement with the overall Düzce fault plot (X in fig. 4.3.4) and an homogeneous trend of the structures. Along the west section, subsections from 1 to 4 show different trends with respect to the overall Düzce fault plot and a more complex pattern of the structures, with meter-scale ruptures and SDZ's that diverge strongly from their PDZ's trends.

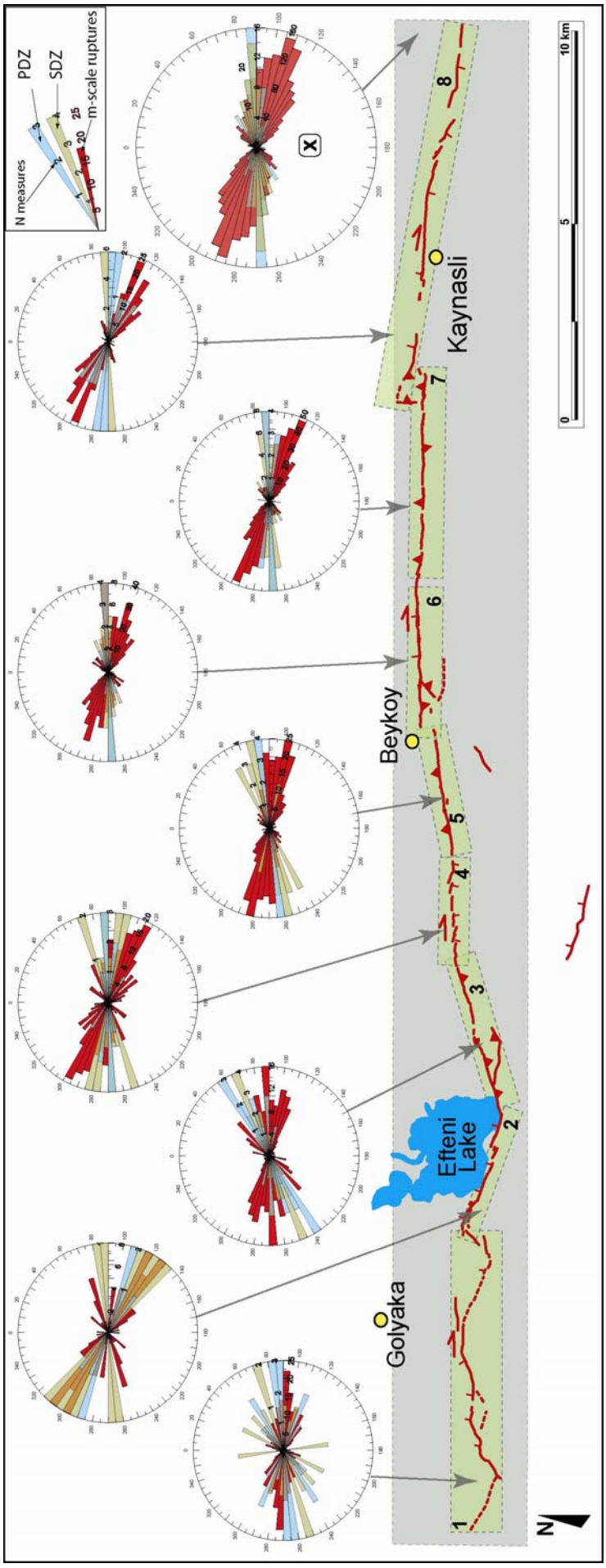

Figure 4.3.4. Rose diagrams of the 1999 ruptures (CFT) trends. Plots show orientation of MSR (red), SDZ (yellow) and PDZ (blue) of different subsections of the Düzce Fault (green boxes). The plot marked with X is referred to the whole Düzce Fault (gray box).

bserving in detail the CFT west section, it is clear that the complexity of the rupture trace is related to the three main families of structures (PDZ) that compose it: the E-W, the WNW-ESE and the WSW-ENE trends. Hence, a further subdivision of the western fault subsections is needed and the related rose diagrams, that group each family trend and dip direction, show: 1) E-W family, with several P-shear-like MSRs and SDZs; 2) WNW-ESE family, with similar SDZs and PDZs and a general convergence of their trends with the MSR trends; 3) WSW-ENE family, with well distinct SDZs and PDZs that form a wider angle with the MSR trends; 4) a reduction of the bimodal distribution of the dip direction of the WSW-ENE family, with preferred northward dip direction (fig. 4.3.5).

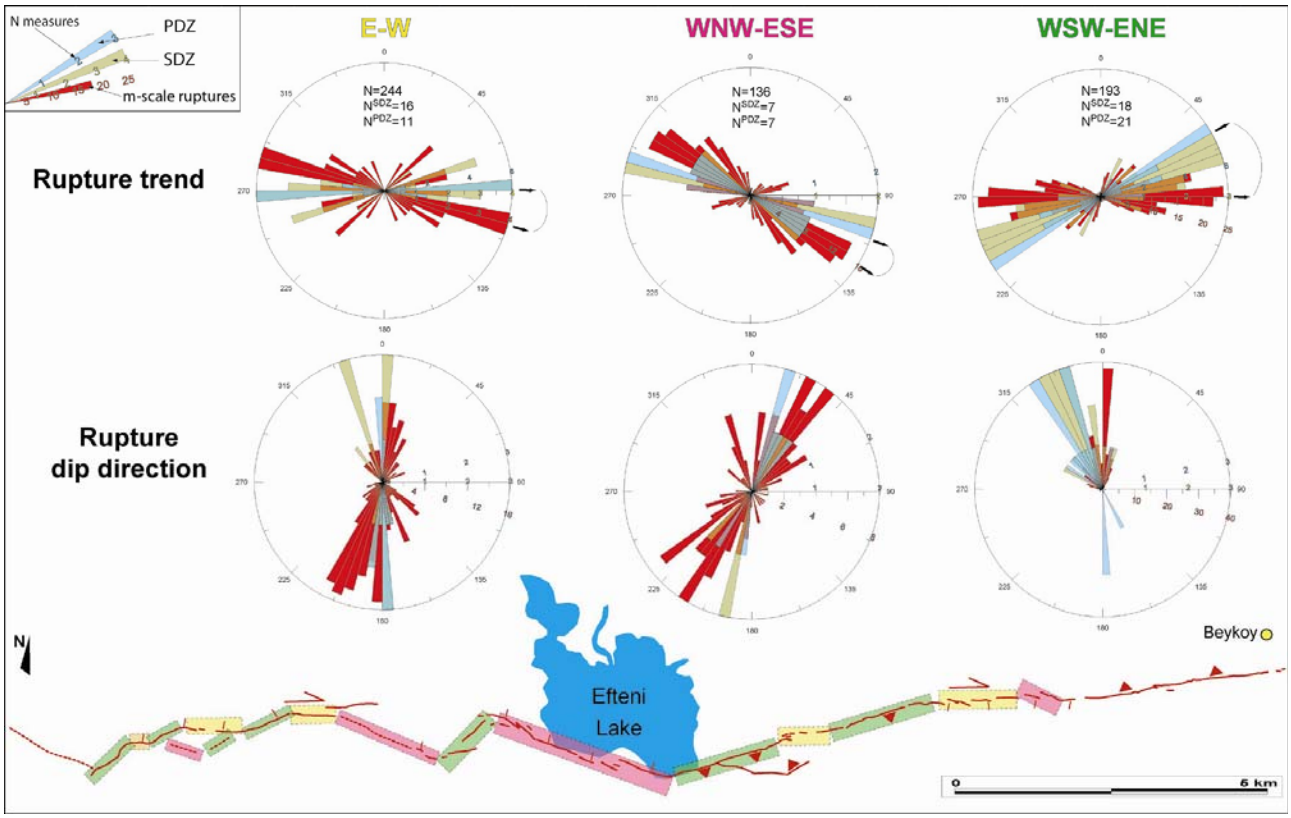

Figure 4.3.5. Rose diagrams of the 1999 ruptures (CFT) trends and dip directions. Plots show orientation of MSR (red), SDZ (yellow) and PDZ (blue). On the CFT, the E-W, the WNW-ESE and the WSW-ENE family trends are evidenced in yellow, pink and green, respectively. Black arrows point the PDZ and MSR average trends.

The average dip-slip component of each subsections was grouped according to their family trend. The mean dip-slip value of each family trend highlights that a slightly larger amount of dip-

slip component was accommodated by the WNW-ESE subsections with respect to the WSW-ENE and E-W subsections (fig. 4.3.6).

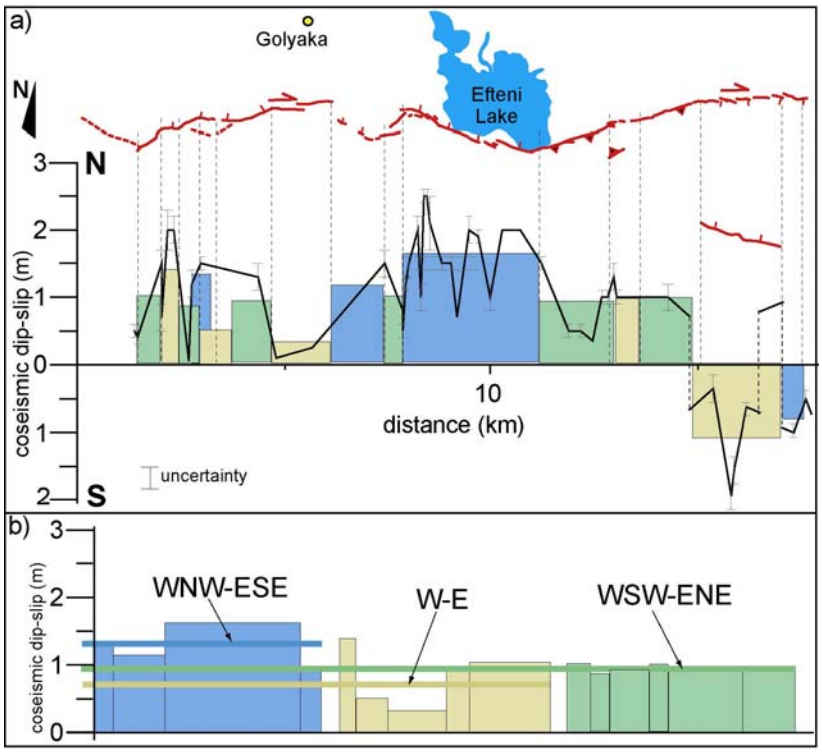

Figure 4.3.6. a) mean dip-slip component for each PDZ. b) average of the dip-slip component for each family trend (solid colored line) of fig. 4.3.5.

Fault data inversion of the CFT of the western section (fig. 4.3.7a and b) indicates a maximum infinitesimal strain axis that forms an angle β of 50° with the E-W trending Düzce fault boundary (fig. 4.3.7c).

The analyzed mole-tracks show variations in the distribution of the push-ups between two consecutive R-shears (see fig. 2.1.5). The percentage of push-ups with respect to the net meter-scale ruptures (MSR) of the mole-tracks is about zero along the WNW-ESE PDZs and increases substantially eastward, up to 36 % east of Beykoy (fig. 4.3.8 and fig. 4.3.9).

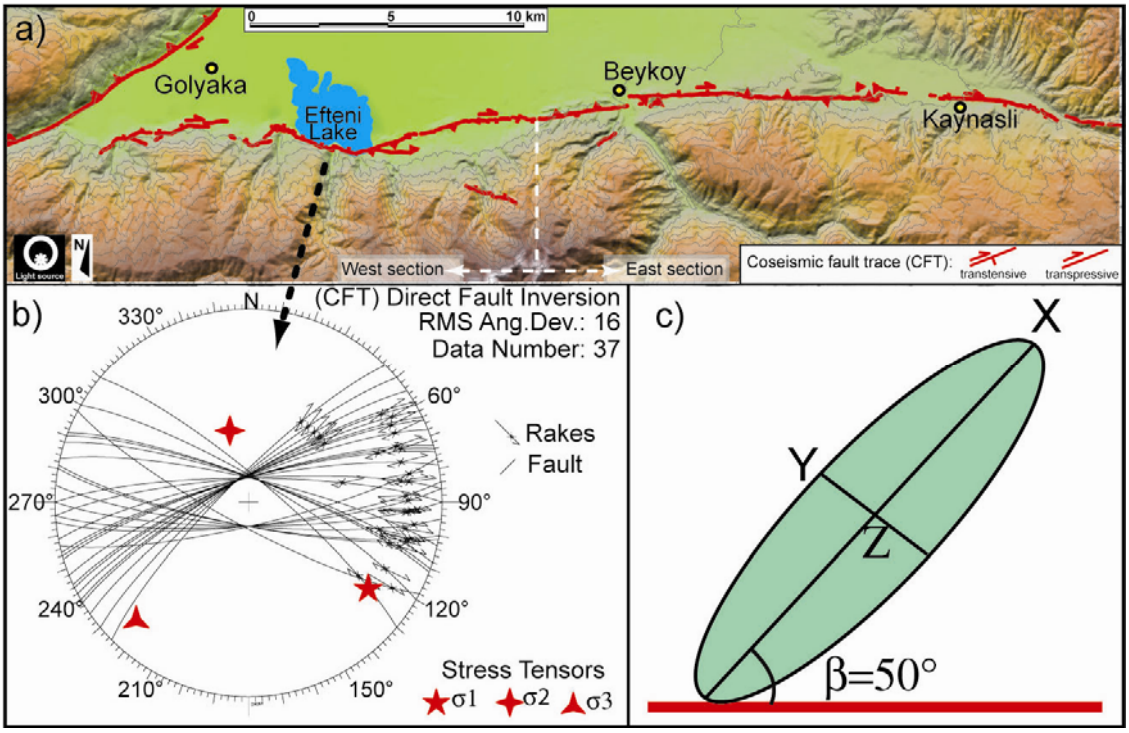

Figure 4.3.7. Analysis of the west section CFT. a) sketch of the CFT of the Düzce area. b) Equal-area stereoplots of the CFT direct inversion of the measured 1999 fault ruptures (lines) and relative rakes (arrows). Calculated stress tensors are shown; c) Infinitesimal strain ellipse of the west section CFT. The angle (β) between the maximum strain axes and the mean fault trend is reported.

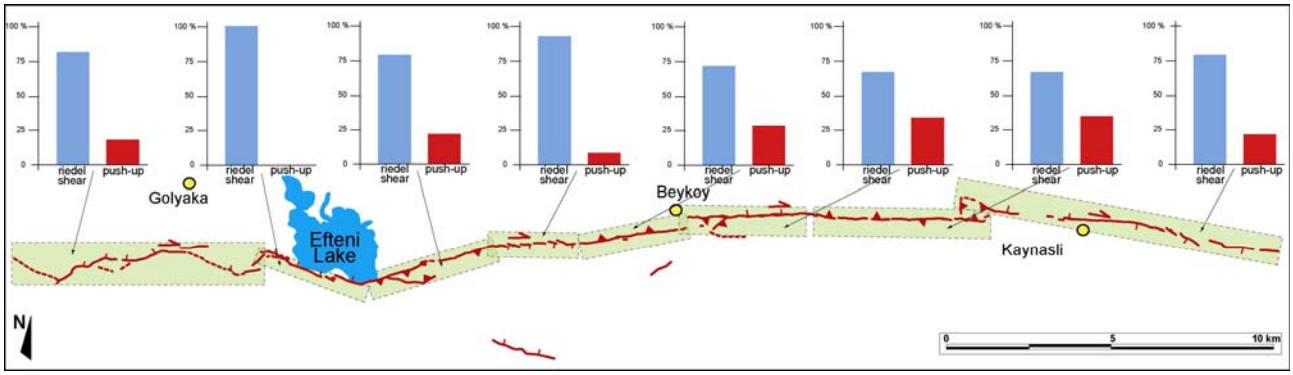

Figure 4.3.8. Histograms of the MSR mole-track components along the 1999 ruptures (CFT). Each graph refers to the percentage distribution of R-shears (blue box) and push-ups (red box) of different elements of the Düzce Fault (green boxes, same as fig. 4.3.4).

Figure 4.3.9. Photos of 1999 coseismic ruptures along the western part of the CFT. Top photos from WNW-ESE trending elements. Bottom photo from WSW-ENE trending element.

4.3.2. The Pliocene-Quaternary fault system (RFS)

The analysis of the long-term geologic and geomorphic setting of the Düzce fault was performed extending the observation in a broader area around the CFT. Structural data (see Appendix I-III) were collected and morphotectonic elements recognized; these describe a long-term kilometric structural pattern, mainly consisting of én-échelon, left-stepping, WNW-ESE striking faults and of right-stepping, WSW-ENE striking faults (fig. 4.3.10). The RFS tectonically controls most of the lithological contacts between the Paleozoic-Eocene bedrock formations (*e.g.*, between formations a, c and e in fig. 4.3.10a); several fault planes outcrop showing dextral strike-slip and, subordinately, oblique kinematic indicators. The RFS can be also traced on the base of evident morphologic lineaments that are not controlled by bedding planes of the bedrock formation since they are differently oriented (see plots of fig. 4.3.10).

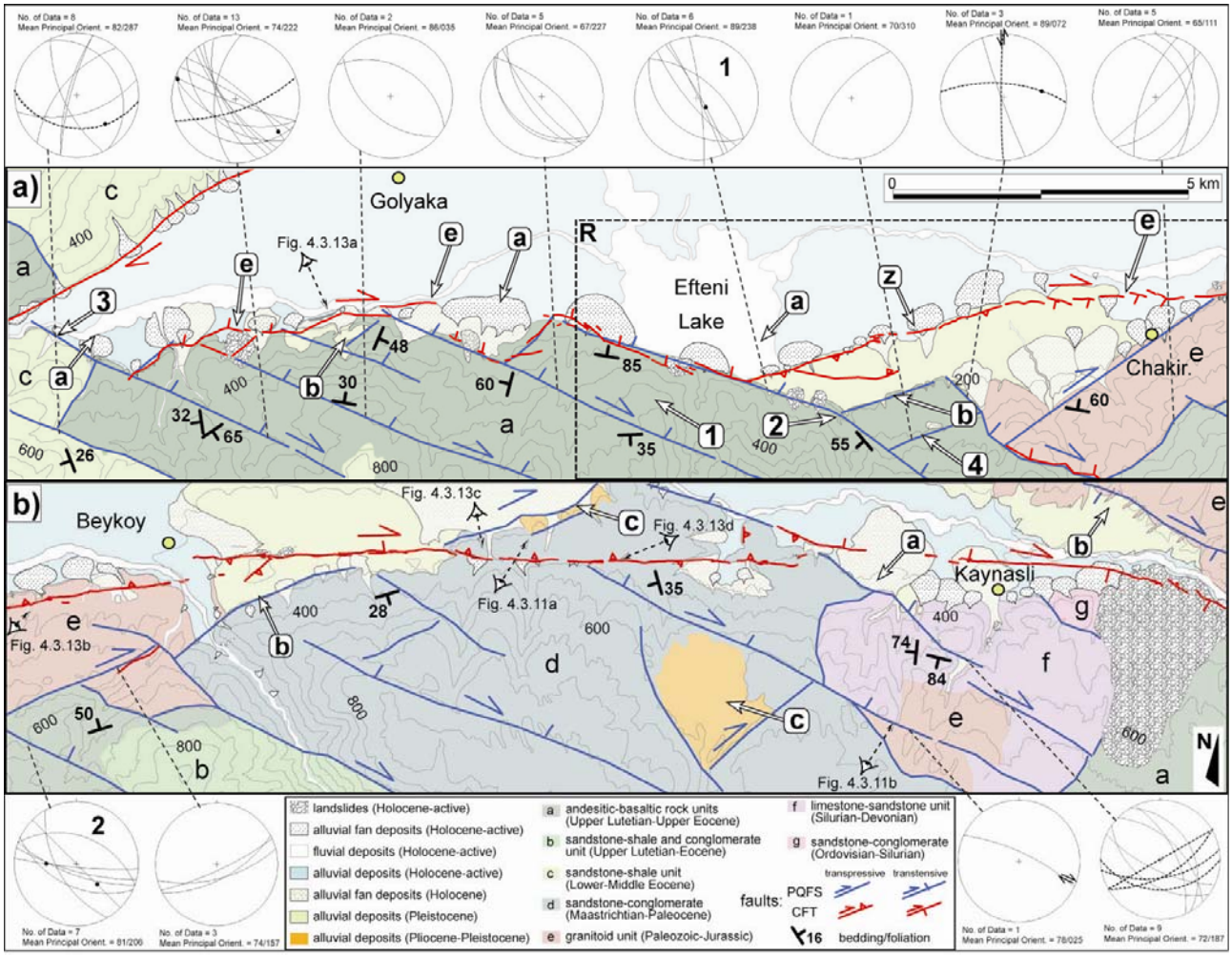

Figure 4.3.10. Geological map of the study area. a) western section and b) eastern section of the fault. Continental deposits from 1:20.000 scale field survey and bedrock units modified from Herece and Akay [2003]. Contour interval 100 m. 1999 ruptures (CFT) and long-term fault system (RFS) are reported. Equal-area stereoplots of the RFS measured fault planes (lines), joints (dashed lines) and relative slickenlines (arrows for clear and points for uncertain kinematics) are shown.

The outcropping WNW-ESE striking faults show some fault planes with dip-slip component of the slickensides (plot 1 and 2, fig. 4.3.10). Also, they have a clear-cut geomorphologic expression with well-aligned linear ridges, saddles and valleys, confirmed by alignments of right-hand deflections of streams (*e.g.*, south-east of Efteni Lake, spot 2 in fig. 4.3.10a). The base of indented and roughly well preserved, up to 250 m high, facets (*e.g.*, south of Efteni Lake, spot 1 in fig. 4.3.10a) along with suspended terraces at the stream outlets (*e.g.*, west of the Golyaka basin, spot 3 in fig. 4.3.10a) and deep stream incisions eloquently depict their transtensive kinematics. Two hot springs along two of the WNW-ESE striking faults suggest that these are rooted to the main fault at depth.

Kinematic indicators were documented on the WSW-ENE striking faults (*e.g.*, fig. 4.3.11a), presenting pure strike-slip slickensides (their transpressive character could be also inferred on the basis of their orientation with respect to the mean Düzce fault motion trend). These faults are also characterized by evident morphologic lineaments, represented by well-aligned linear ridges, saddles and valleys along with abrupt slope gradient changes (spot 4, fig. 4.3.10a), evidence of important vertical movements.

The activity of RFS during the Pliocene-Quaternary deformational history of the Düzce fault is clearly expressed by its control on the continental sediment deposition between the range front, to the south, and the basin infill, to the north (fig. 4.3.10 and Plate 1a). The RFS bounds the triangular embayments in the range front, filled by Holocene fluvial deposits (spots a in fig. 4.3.10), Pleistocene alluvial fans (spots b in fig. 4.3.10) and, locally by Late Pliocene-Early Pleistocene conglomerate-sandstone units (spots c in fig. 4.3.10b and fig. 4.3.11b), shed from the southern highlands [Emre et al., 1998]. Another clear evidence of the control of the RFS on the present geomorphology is provided by the Kaynasli lozenge-shaped basin located in the eastern part of the fault. Pull-apart opening and the preservation of Late Pliocene-Holocene deposition in this basin has been controlled by two WNW-ESE main left-stepping Riedel shears that are part of the RFS (fig. 4.3.12).

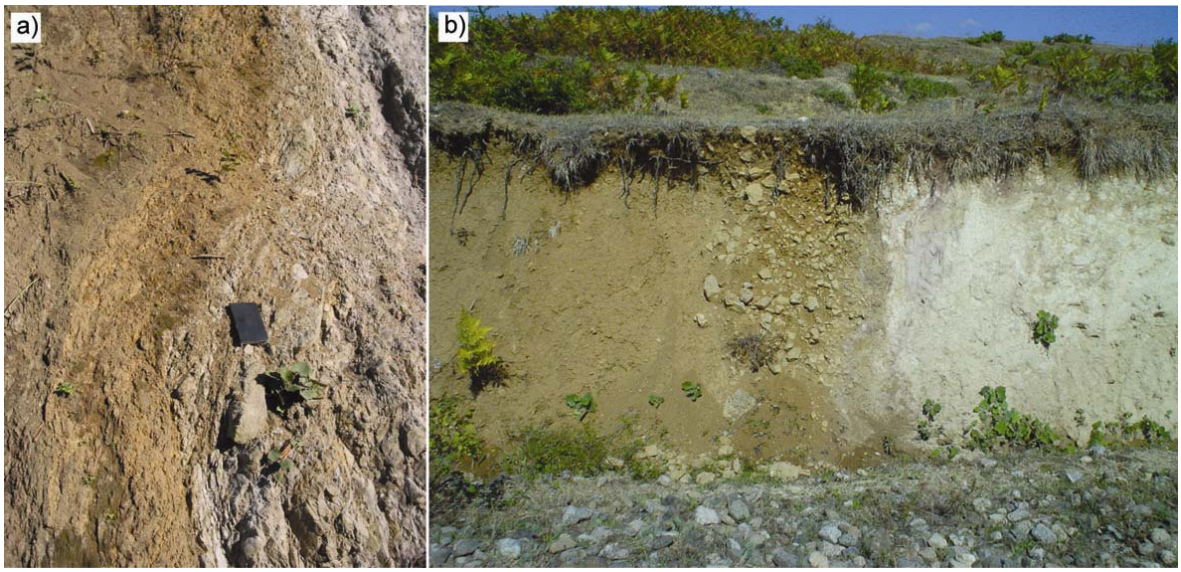

Figure 4.3.11. a) photo of a RFS shear zone affecting the bedrock formations; b) photo of a tectonic contact, part of the RFS, between continental deposits and bedrock. (see fig. 4.3.10b for locations).

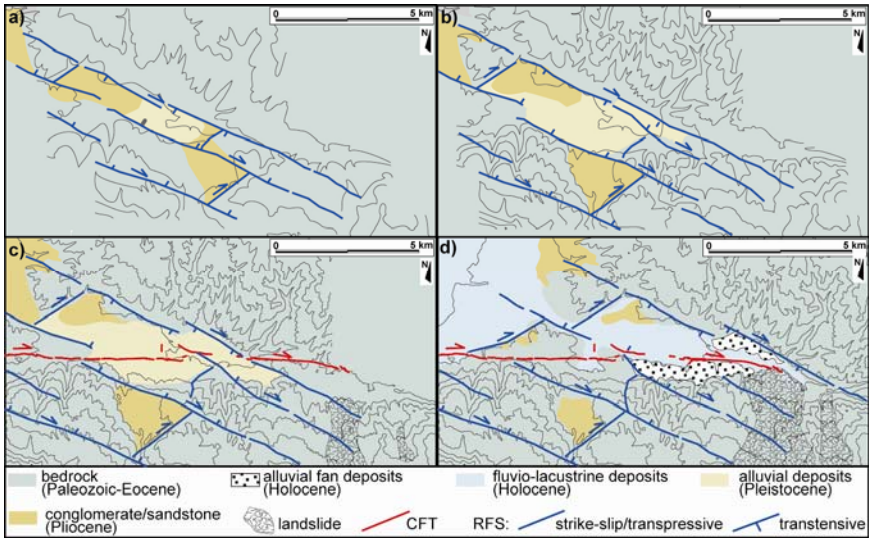

Figure 4.3.12. Conceptual model of Kaynasli basin evolution. a-b) Pleistocene, the pull-apart basin opens due to the RFS activity; c-d) Pleistocene-present, CFT cross-cut the RFS.

4.3.3. CFT versus RFS

The comparison of the CFT and the RFS highlights that the Düzce Fault is composed of two different sections where: the CFT is strongly controlled by the RFS setting, in the western section (fig. 4.3.10a), whereas the CFT cuts across the RFS features and assumes a quite linear, independent trajectory, in the eastern section (fig. 4.3.10b).

The western section of the CFT has a saw-tooth arrangement with changes of trajectory mainly following *en échelon* left-stepping, WNW-ESE striking, and right-stepping, WSW-ENE striking, subsections that reactivated the RFS. In Chapter 4.2 the easternmost part of this section (R in fig. 4.3.10) were investigated and the relationships between the coseismic and the old fault systems were analyzed. Here, has been observed that the fault developed a young WSW-ENE and E-W fault system (spot z in fig. 4.3.10) that abandoned, probably during the Late Pleistocene, the rangefront-bounding faults. Conversely, along the westernmost part of this section, the saw-tooth arrangement of the CFT contains prevalent WNW-ESE and WSW-ENE striking subsections and secondary, few E-W trending subsections. The WNW-ESE and WSW-ENE striking subsections are associated to mature short/long-term landforms, such as suspended terraces (fig. 4.3.13a) that suggest a persistent dip-slip component of the fault motion.

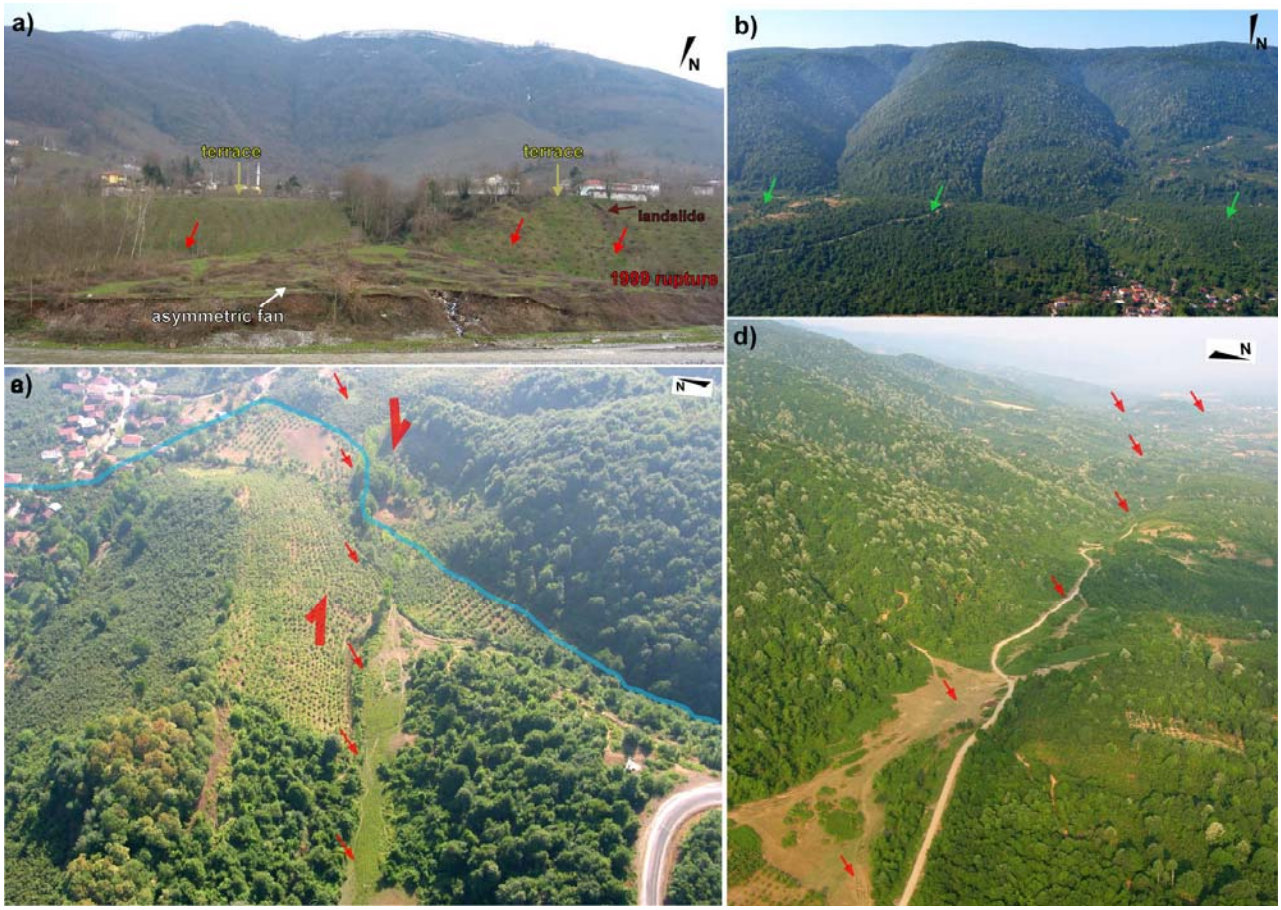

Figure 4.3.13. Geomorphic expressions of the CFT. a) fault scarp due to the dip-slip component. White open arrows point to the 1999 ruptures, solid arrows point to the terrace and to the outlet of the entrenched stream that form the asymmetric alluvial fan, due to the right-lateral fault motion; b) Aerial view of the drainage controlled by the shutter ridges (white open arrows); c) Aerial view of a stream (white line) deflected about 100 m by the short-term activity of the right-lateral fault motion (black arrows); d) Aerial view of the linear valley along the fault trace (black arrows). (see fig. 4.3.10. for locations).

Differently, the E-W trending subsections (spots e in fig. 4.3.10a) are associated to subtle and youthful short-term landforms, including both fault scarps and pressure ridges. These subsections, which hosted a limited cumulative deformation, may represent an incipient stage of evolution of the fault system from saw-tooth to linear geometry.

In contrast, the CFT has completely overcome and cut the RFS in the eastern section. Here the CFT shows a regular E-W trajectory, parallel to the mean trend of the seismogenic Düzce fault, is associated with a prominent morphological imprint, highlighted by large drainage dislocations (fig. 4.3.13b), entrenched fault-parallel linear valleys (fig. 4.3.13c), and well developed shutter ridges (fig. 4.3.13d). All this indicates the CFT's persistent short/long-term activity with mostly pure strike and, only locally, transpressional slip. The E-W trending subsections of the eastern CFT,

that exhibit well developed landforms, show a marked difference with respect to the few E-W trending subsections of the western CFT, which have a weak short/long-term geomorphic expression and thus accumulated a lower displacement (see Plate 1).

4.3.4. The overall long-term morphological expression

The 1:25,000-scale geological and geomorphological map of the Düzce Fault (Plate 1a and simplified map of fig. 4.3.14) shows landforms, related to the erosional and the depositional processes that have been shaping the Almacik range-front, strongly coupled with near-fault tectonic landforms related to fault location and activity.

The erosion of the Almacik block provided most of the sediment production for the Düzce Basin. These sediments that cover the foot of the range-front mainly coalesce in bajadas (similar to the one observed in detail in Chapter 4.2.2) composed of Middle-Late Pleistocene alluvial fan and Late Pliocene-Early Pleistocene conglomerate-sandstone units (zone x, fig. 4.3.14) [Herece and Akay, 2003], and also of active Holocene fans, deposited in subsequent incisions of the old bajadas (spot y, fig. 4.3.14). The generally loose and soft recent deposits recorded persistent landform modification due to faulting and developed well-expressed tectonic-related morphologies whose topography controlled the drainage pattern. Such tectonic-related morphologies are clearly not related to the dynamics of the bajada, since they deform the original depositional layers (fig. 4.3.15). The most common tectonic landforms in the study area are: tilted surfaces, fault escarpments, benches, saddles alignments, linear valleys, shutter ridges, pressure ridges, and sag ponds (fig. 4.3.14).

Although the overall long-term morphological expression depicts the Düzce fault, from the Karadere section to east of Kaynasli, as a single and continue structural element, it presents internal differences,.

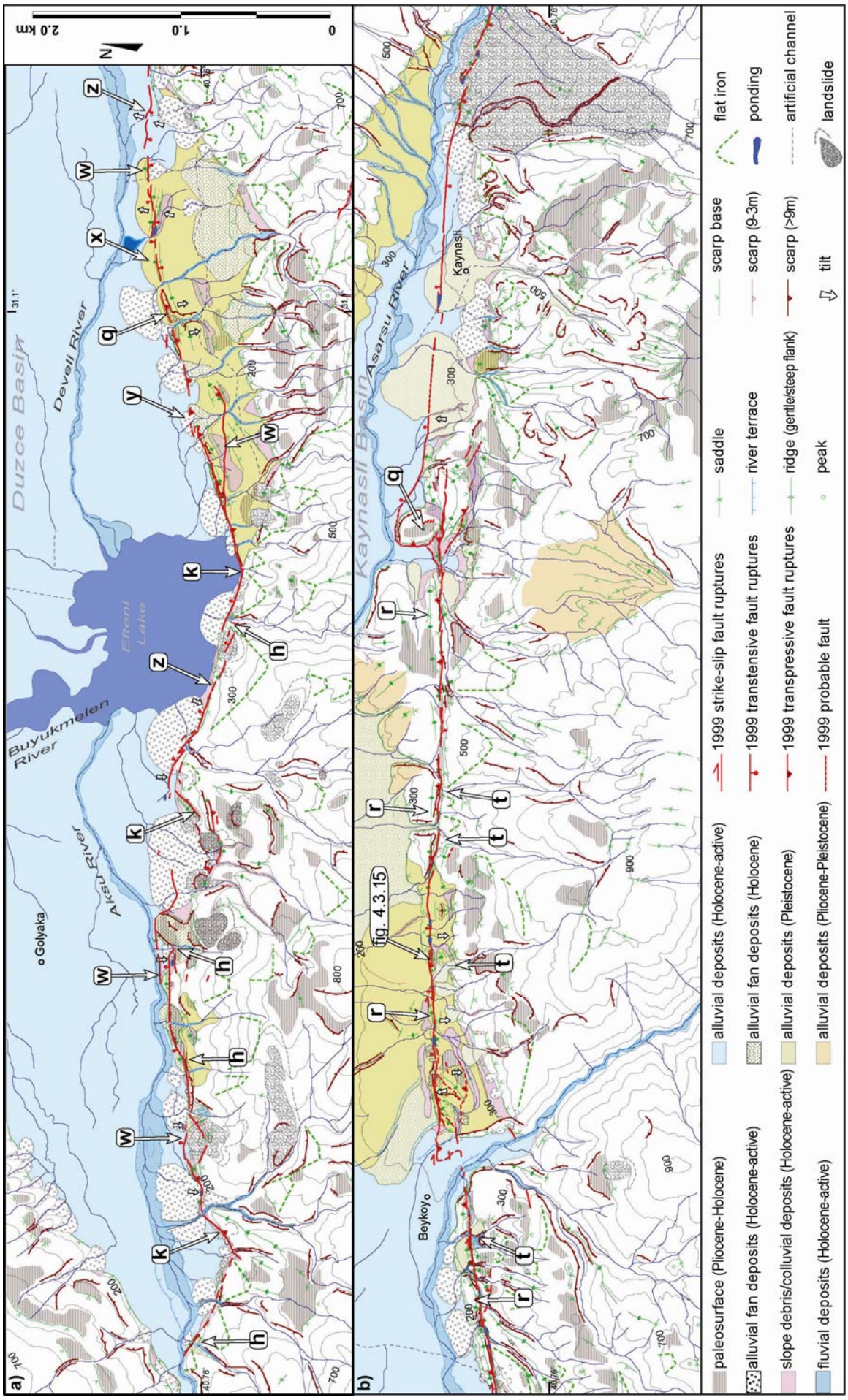

Figure 4.3.14. Simplified geomorphological and coseismic fault scarp map of the two parts of the Düzce Fault. a) Western section. b) Eastern section. Continental deposits from 1:20 000 scale field survey, bedrock from Herece and Akay [2003]. Letters indicate locations discussed in the text. Contour interval 100 m.

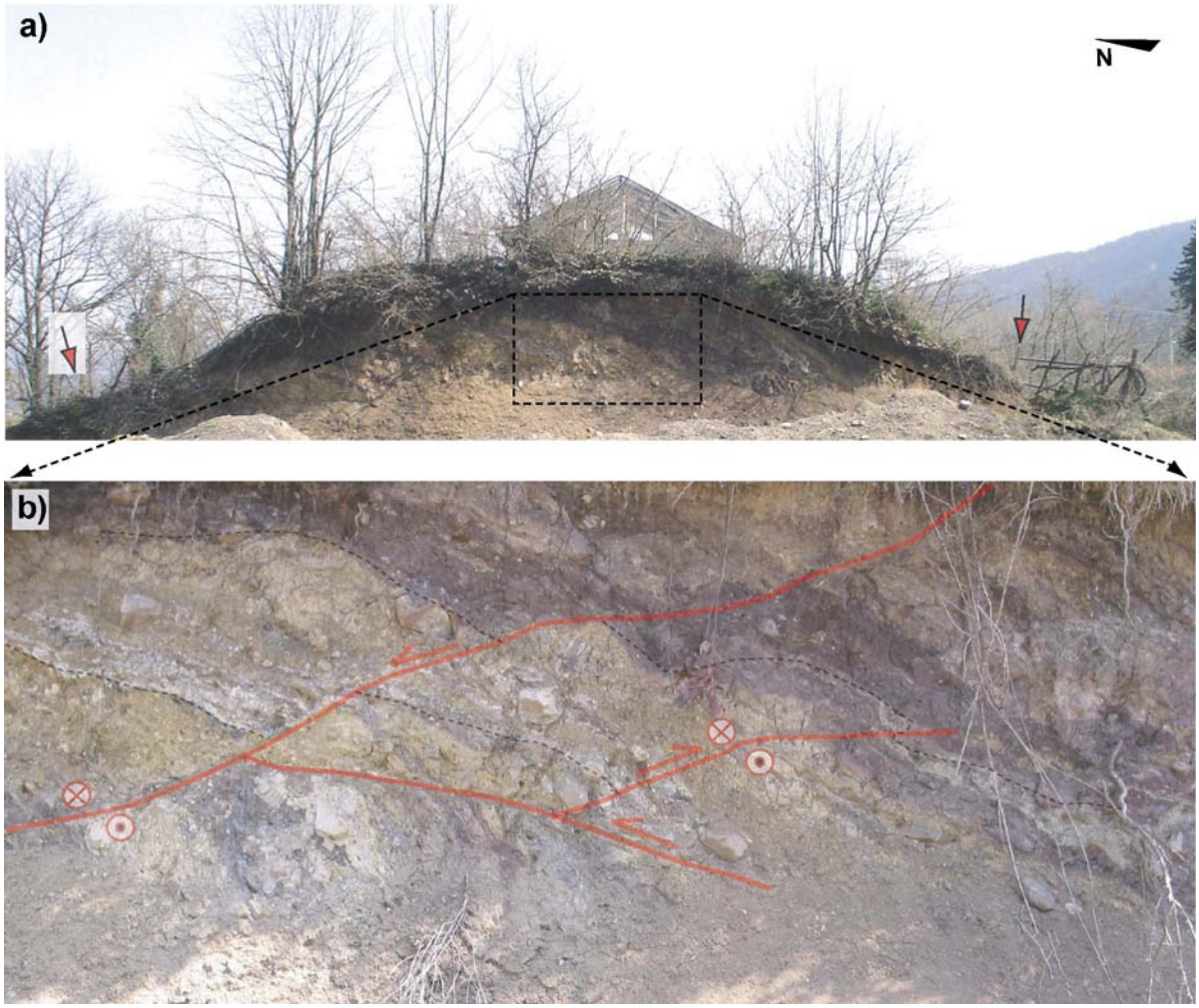

Figure 4.3.15. a) View of a cross-section of a tectonic ridge along the Düzce Fault. Red arrows point to the 1999 ruptures. b) Close up of the deformed Quaternary fan deposits outcropping at the tectonic ridge. The deformation zone mainly shows transpressional structures with apparent transtensional structures caused by the juxtaposition of the strike-slip motion. Dotted circle indicate the block moving out of the picture. (see fig. 4.3.14 for location).

Along the western section of the Düzce fault, the 1999 coseismic fault trace (CFT) bounds the triangular embayments of the range front, that host bajadas. As already mentioned, the rupture follows mainly a saw-tooth trajectory (*e.g.*, spots k, fig. 4.3.14a) associated with linear escarpments and strong stream incisions south of the CFT. Holocene suspended terraces (up to 20m) can be found at the stream outlets along the range-front foot (spots h, fig. 4.3.14), that, together with back-tilted surfaces at base of the range front, suggest an important subsidence north of the Düzce Fault. The few E-W trending elements (*e.g.*, spots w in fig. 4.3.14a), associated to subtle and youthful landforms, suggest they have hosted only a small cumulative deformation.

Conversely, the eastern section of the Düzce Fault (fig. 4.3.14b) presents a more regular, localized, prominent E-W trace parallel to the mean trend of the whole Düzce fault. This E-W trending section crosscuts both recent continental deposits and bedrock and is associated with well developed landforms indicating its persistent long-term activity. It is characterized by shutter and pressure ridges, 300 to 1000 m-long, up to 120 m high (*e.g.*, spots r, fig. 4.3.14b), with elongated shapes and long axes paralleling the escarpment elements they are associated with. In many cases, the ridges act as natural dams for northward flowing drainages, being thus responsible for the formation of ponds and the trapping of Holocene fans against the scarp (*e.g.*, spots t, fig. 4.3.14b). Only the easternmost part of this E-W trending section shows subtle near-fault tectonic landforms, going through the Holocene deposits of the Kaynasli pull-apart basin.

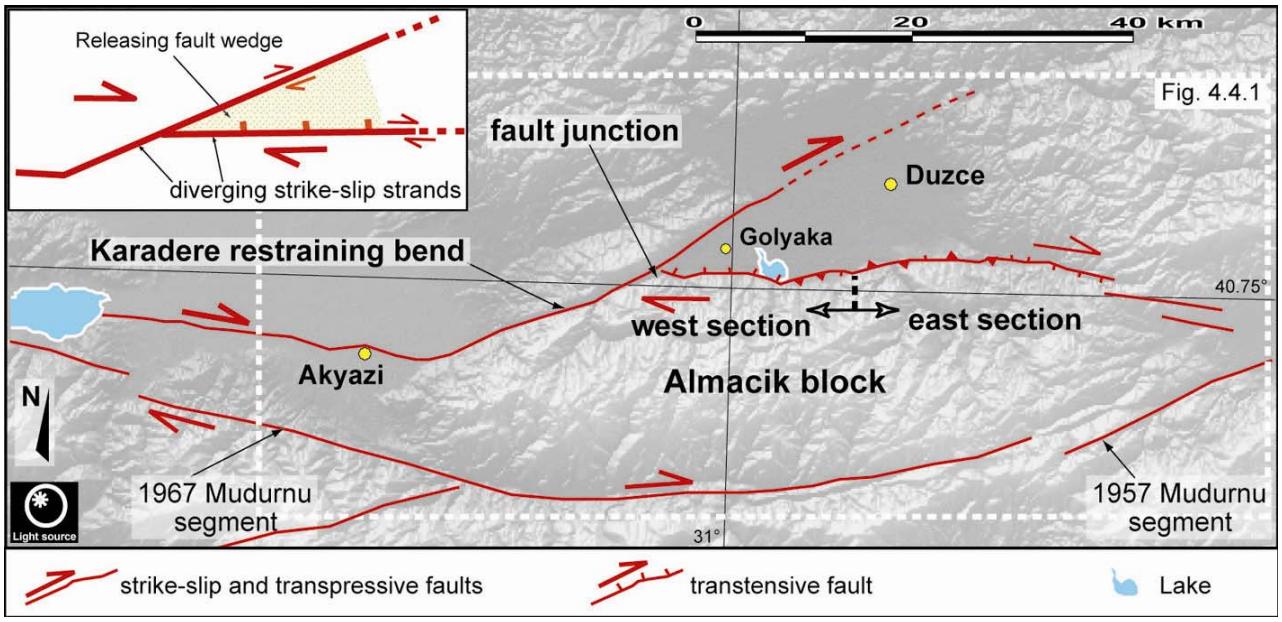

Figure 4.3.16. Schematic structural map of the North Anatolian Fault in the Düzce region. The SW-NE striking Karadere section represents a restraining bend of the Izmit segment, that bifurcates and links to the westernmost part of the Düzce segment by a fault junction. The inset shows a simplified sketch of the fault junction between Karadere section and Düzce faults [modified from Christie-Blick and Biddle, 1985].

The area of investigation was extended to the west, because of the geometrical setting of the Düzce Fault with respect to the Karadere fault section. This may be suggestive of a strict interaction between them. Observations on the relationships among the Karadere restraining bend, the Düzce fault and the Düzce Basin were collected. The Karadere section and the Düzce fault are two

diverging strike-slip strands that are linked by a fault junction (*sensu* Christie-Blick and Biddle [1985]) and not as a step over. This geometrical array configures a releasing fault-wedge whose long-term morphological expression is represented by the wedge-shaped basin of the Golyaka area (fig. 4.3.16). Here, the vertical component of the movement strongly controls the drainage system. In fact, in the Düzce Basin, the streams arrangement has a centripetal pattern, converging to the present basin depocentre, the Efteni Lake (fig. 4.3.17a and b). This depocentre has been migrating from the central part of the basin southwestward [Kazancı et al., 2003], migrating 7 km in ca. 2.5 My, as testified also by the basin infill thickness (fig. 4.3.17c). The only stream that drains the Efteni Lake, flows northward and crosses orthogonally the Karadere restraining bend. This latter is responsible for the north-eastward transpressional motion and growth of the Karadere ridge, in fact it dams and pushes the north-flowing stream, as testified by paleo-valleys and wind-gaps (spot x in fig. 4.3.17a and fig. 4.3.18), and it deforms the Düzce Basin deposits creating the gentle threshold for the stream flow, as highlighted by the DEM (spot y in fig. 4.3.17b). For these reasons, only the westernmost part of the Düzce Basin in the Golyaka area, is the present-day fault-related floodplain. The northern part of the basin is inherited and no more active.

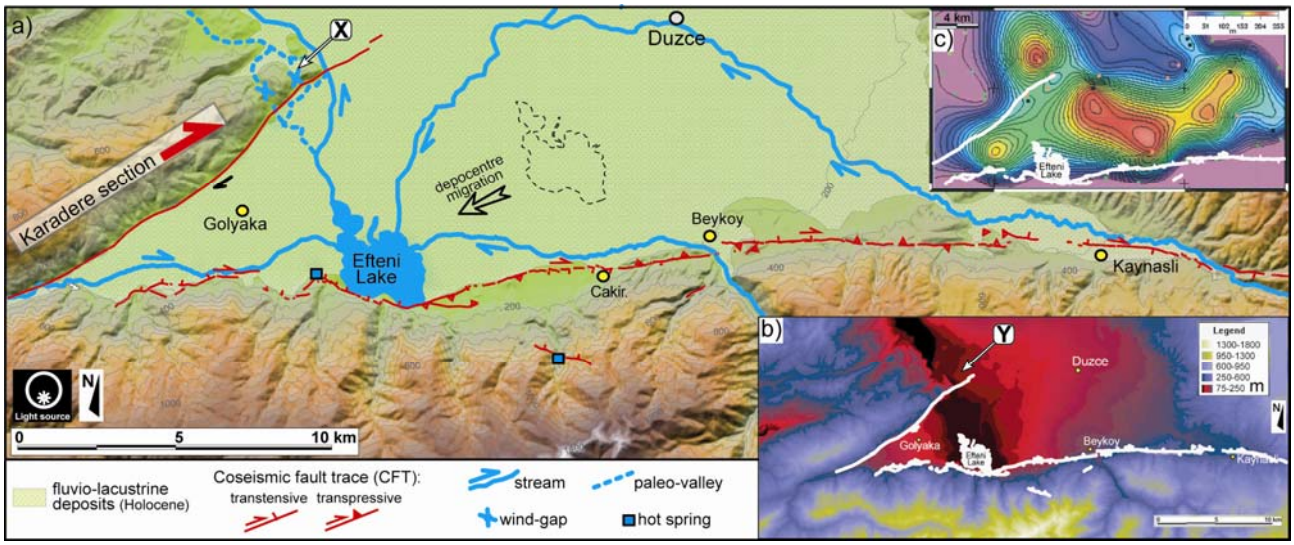

Figure 4.3.17. Sketch of the relationships between 1999 ruptures (CFT) and main drainage features of the Düzce basin. Shaded relief based on digital elevation model (DEM, interpolated from 10 m contours and auxiliary 5 m contours of 1:25.000 scale topographic maps). Contour interval 100 m. Inset shows the strain ellipse related to the shear couple of the Düzce master fault (red arrows), trend of structures related to its extensional and compressional components (black arrows) are reported.

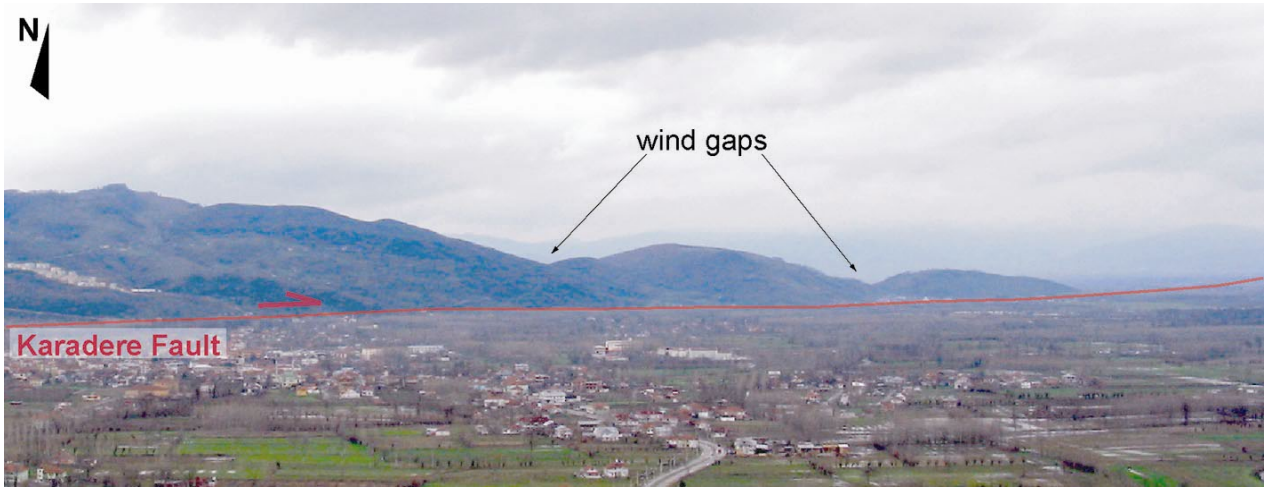

Figure 4.3.18. Panoramic view of the Karadere fault section bounding the Düzce Basin in the Golyaka area.

4.4. The interaction between the Düzce and Karadere fault sections

The right-lateral coseismic slip distribution at the surface and the overall long-term morphology suggest that the Düzce fault is a continuous fault segment that splays out from the releasing junction with the Karadere section (fig. 4.3.15). Although it exhibits such a continuity, it has been defined a clear difference in the setting and in the overall fault-related long-term morphology of its eastern and western parts. The question is now to understand what can be the cause of this difference. The junction between the Karadere and Düzce faults represents a clear singularity in the geometrical arrangement in this part of the NAFZ. Under this light, if the landscape of the westernmost part of the Düzce Basin derives from the accumulation of repeated 1999-type earthquakes was tested. For this purpose, the observed basin morphology were compared with the coseismic deformation field.

	Strike	Dip	Rake	slip	Lenght	Depth extent [1]
Düzce Fault	268° [2]	73° [2]	177° [2]	3.0 m [6]	40 km [2]	0-17 km
Karadere section	243° [3]	70° [3]	5° [4]	2.5 m [7]	45 km [3]	0-17 km
1967 Mudurnu segment	278° [5]	85° [5]	5° [5]	2.5 m [8]	80 km [5]	0-17 km
1957 Mudurnu segment	254° [5]	78° [5]	180° [5]	2.0 m [8]	40 km [5]	0-17 km

Table 4.4.1. Parameters of the fault models utilized for the elastic dislocation calculations: [1] on the basis of aftershocks distribution [Ambraseys and Zatopek, 1969; Tibi et al., 2001; Özalaybey et al., 2002] and maximum depth for coseismic slip from GPS inversion [Reilinger et al., 2000] and GPS, InSAR and Spot data [Delouis et al., http://www.seismo.ethz.ch/srcmod; Feigl et al., 2002; Çakir et al., 2003a and 2003b]; [2] USGS; [3] on the basis of aftershocks distribution [Ben-Zion et al., 2003; Iio et al., 2002] and surface geology [Emre et al., 2003]; [4] on the basis of static stress analysis [Muller and Aydin, 2004] and surface geology [Emre et al., 2003]; [5] on the basis of focal mechanisms [McKenzie, 1972; Canıtez, 1972] and surface geology [Ambraseys and Zatopek, 1969; Barka, 1996]; [6] on the basis of rupture models from geodetic [Bürgmann et al., 2002; Çakir et al., 2003a] seismological [Birgören et al., 2004] and joint inversion analysis [Delouis et al., http://www.seismo.ethz.ch/srcmod]; [7] on the basis of rupture models from geodetic analysis [Reilinger et al., 2000; Feigl et al., 2002; Çakir et al., 2003b]; [8] from seismic moment estimations [Pinar et al., 1996; Muller et al., 2003; Stein et al., 1997].

The expected coseismic deformation field were modeled by using a standard dislocation code developed by Ward and Valensise [1989]. To get a complete image of the fault related landscape, also Mudurnu 1967 and Mudurnu 1957 earthquake segments, which may have also a role in shaping the study area (see Chapter 3.2.2, fig. 3.2.14), were introduced in the model, together with the Düzce and Karadere 1999 fault segments. Planar, rectangular faults, embedded in an elastic half-space with uniform slip were assumed. To simplify, slip during the most recent earthquakes on these faults (*i.e.*, 1999, 1967, 1957) is considered characteristic [Schwartz and Coppersmith, 1984]. The modeled fault parameters (fig. 4.4.1), were derived from available coseismic seismological, geodetic and geological observations and are summarized in Table 4.4.1.

Two maps, one for the vertical and the second for the N-S component of surface deformation, respectively (fig. 4.4.1), were reconstructed from the resulting dislocation model. Obviously, modelling faults as boxes and assuming characteristic and uniform slip, without any tapering off at fault tip lines, are oversimplifications. Nevertheless, with exception for some minor mismatches (*e.g.*, subsiding portion of the northern block of the Karadere section) and discrepancies that may depend on inheritance from the previous compressional phases [Şengör et al., 1985], the

maps show how the repetition of earthquakes on the four modeled faults contributed in building up the present long-term topography of the study area.

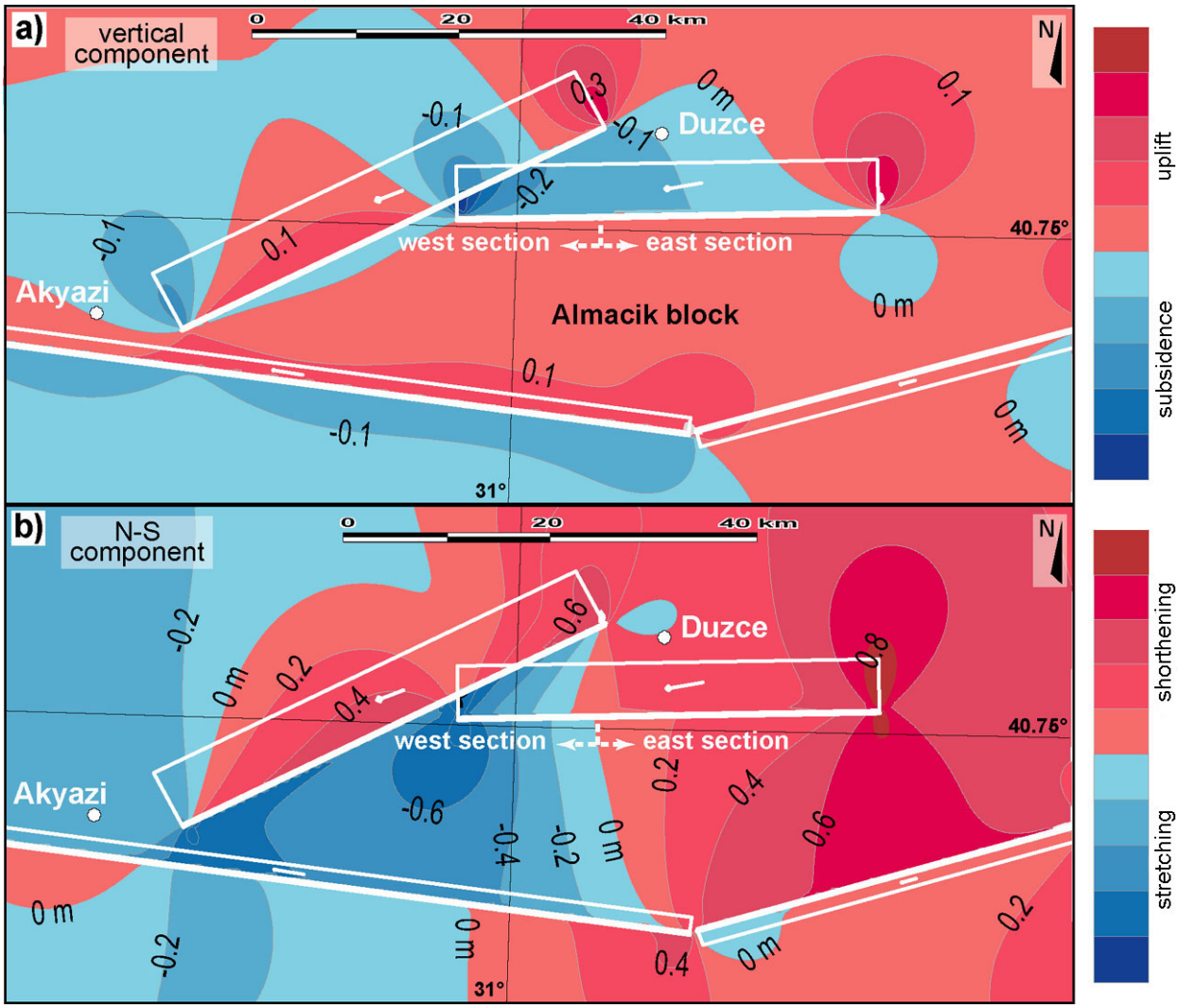

Figure 4.4.1. a) Vertical component of elastic dislocation modeled for the North Anatolian Fault array of the study area. The boxes correspond to the projection at the surface of the Düzce, Karadere and 1967 and 1957 Mudurnu fault planes (see text and tab. 4.4.1 for details). Contour interval 0.1 m. b) N-S horizontal component of elastic dislocation (same fault array than -b- see text for details). Contour interval 0.2 m. (see fig. 4.3.15 for locations).

Figure 4.4.1 shows: 1) uplift of the Almacik block; 2) subsidence of the Akyazi basin; 3) uplift of the northern part of the Düzce Basin with maxima located at the north-eastern tip of the Karadere fault; 4) subsidence of the Golyaka fault-wedge basin, in coincidence with the present active floodplain, with maxima at the western tip of the Düzce fault; 5) maximum N-S stretching across the western section of the Düzce fault.

4.5. Discussion

In order to understand if there is any space and time evolution of the fault pattern at the surface that can be deciphered, a comparison between the coseismic and the short/long-term data-sets has been accomplished, both alongside the key area and the whole Düzce fault.

4.5.1. Insights from the key area

The comparison between the coseismic and the short/long-term data-sets has been accomplished both along the 1999 coseismic ruptures (hereinafter referred as near-fault) and on the ~4 km wide area along the coseismic fault trace (hereinafter referred as near-fault).

4.5.1.1. Coseismic ruptures vs. short/long-term tectonic landforms in the near-fault

A general coherence at the scale of principal displacement zone (PDZ), both in location and relative movement, between the 1999 coseismic fault trace and cumulative tectonic landforms along it, has been identified (fig. 4.5.1a). The PDZ closely mimics the short/long-term, fault-related morphologic pattern. Also, the location and distribution of the PDZ vertical component of displacement appear to correlate well with the cumulative tectonic landforms, emphasizing the pre-existing relief (*e.g.*, x in fig. 4.5.1a). On the contrary, at a larger scale (SDZ and larger, see fig. 4.2.4), the subordinate coseismic structures diverge from the short/long–term morphologies: the en-échelon ruptures arrays generally “climb” diagonally across the landforms (*e.g.*, fig. 4.5.2).

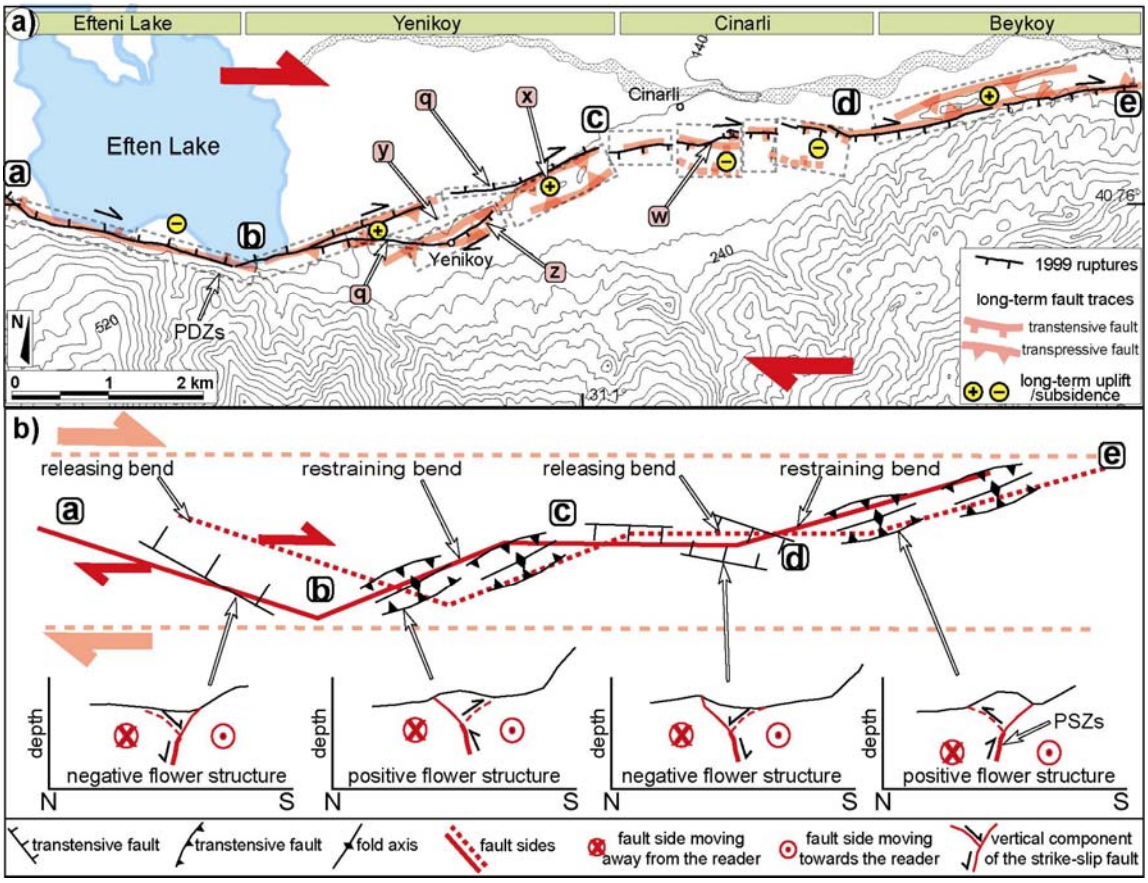

Figure 4.5.1. a) Comparison of the 1999 coseismic ruptures and the fault trace inferred from cumulative tectonic landforms in the near-fault (see text for explanation). Contour interval 20 m. b) Sketch showing the coherence between restraining and releasing bends of the 1999 coseismic ruptures (a-b, b-c, c-d and d-e subsections) and the location of typical cumulative tectonic landforms. Simplified cross sections for each fault subsections are shown. Big red arrows show the shear couple of the Düzce fault. Little red arrows show relative movement, both coseismic and long-term, of the two fault sides (dashed and continuous red lines).

Figure 4.5.2. Photo of the en-échelon SDZs climbing the escarpment near Yenikoy (photo taken soon after the earthquake).

The only relevant incoherences between the coseismic fault trace and cumulative tectonic landforms recognized at the scale of the PDZ are found at the Yenikoy and Cinarli subsections. In the first case, on the basis of cumulative tectonic landforms, a right-step between long-term transpressive fault structures (y in fig. 4.5.1a) that was violated by two coseismic ruptures, has been identified (q in fig. 4.5.1a), linking the right step-over and forming a duplex. The two, E-W trending, linkage ruptures are associated with a cumulative tectonic relief much lower than that of the two main transpressive fault structures. This suggests that the linkage ruptures may be: 1) secondary transfer structures; 2) pure strike-slip elements with no vertical offset; 3) late Y-shear-like features. In the other case, along the Cinarli subsection, one of the cumulative major fault scarps was not entirely reactivated and the rupture cross-cut the morphological warp linking two consecutive left stepping scarps (w in fig. 4.5.1a).

The good correlation between 1999 ruptures at the PDZ scale and cumulative tectonic landforms in the near-fault indicates a persistent location of the fault trace and style of deformation through several seismic cycles. However, apart from the Efteni Lake subsection, the 1999 ruptures represent only a part of the fault pattern inferred from cumulative tectonic landforms (and thus of the PDZ). The overall long-term deformation zone in the near-fault (fig. 4.5.1a) appears not only wider but also more complex than the coseismic one, including other fault strands to the south and/or to the north, which did not rupture in 1999. This raises the possibility that secondary structures have hosted relatively small, blind displacements or rupture only rarely the surface. In one case coseismic ruptures (near Yenikoy, z in fig. 4.5.1a) occurred along these secondary structures and described a PDZ up to 500m wide. These secondary coseismic ruptures demonstrates a superficial anastomosing of the fault system that contributes to the growth of tectonic landforms together with plastic deformation of loose deposits. In fact, as discussed by Sibson [2003] (see Chapter 2.1.5), the width of the deformation zones at the surface (corresponding to PDZ in this Thesis) is mainly related to the presence of young cover sequences of alluvium and to free surface effects. The PDZ appears to be the surface expression of a localized slip plane at depth (hereinafter

PSZ, principal slip zone; see fig. 4.5.1b), as observed along other seismogenic structures (*e.g.*, Landers [Sieh et al., 1993; Jhonson et al., 1994; Lazarte et al., 1994]; Dast-e Bayaz [Tchalenko and Ambraseys, 1970; Tchalenko and Barberian 1975]). This implies that measures along the 1999 surface ruptures could underestimate, although in a minor part, the total amount of the coseismic slip.

Although at the outcrop scale the SDZs outline the fault location, they cannot unequivocally be indicative of the kinematics of the fault subsections. An enlarged distribution of R-shears or push-ups is suggestive of transpression or transtension, respectively. In general, the mole tracks ruptures, that typify the 1999 rupture style, advise whether the relative uplift of the two fault blocks is due to a compressional or extensional component of displacement, but the cumulative tectonic landforms express clearly the local stress fields of the four fault subsections. The fault subsections reflect tectonic landforms according to strike-slip movement along an irregularly curved fault that produces transtension at releasing bends and transpression at restraining bends (fig. 4.5.1b). In fact, the E-W trend of the dextral Düzce shear couple tends to create a local transtensional strain field along Z-shaped fault trajectories and a local transpressional strain along S-shaped fault trajectories. The morphology of the Efteni lake fault subsection fits well with a normal component of the fault motion. The strike of the Yenikoy and Beykoy subsections suggests a local transpressive strain field, which is compliant with the observed right-stepping pressure ridges (the surface expression of cumulative positive flower structures). The coseismic rupture along the Beykoy subsection shows a lowering of the southern block. These local displacements reflect the growth of the pressure ridges of these subsection and do not exclude the uplift of the Almacik block with respect to the basin as depicted by geodetic data. The Cinarli subsection shows a gentle negative flower structure, in accordance with the fact that it only slightly deviates from the average trend of the Düzce fault. This gentle flower structure affects the bajada forming local basins (fig. 4.5.1b).

Summarizing, in the near-fault, the observed coseismic and short/long-term structures (PDZ) show vertical tectonic component that is related to local change of the fault trajectory. This

geometrical complexity produces subsidiary folding and thrusting with small wave-length (less than 1 km) that suggests they are shallow-rooted to the same master fault (see Chapter 2.1.6).

4.5.1.2. Coseismic ruptures vs. short/long-term tectonic landforms in the far-field

Examining the broader area around the coseismic ruptures we have seen that, with the exception of the Efteni Lake subsection, the RFS and the 1999 fault subsections (CFT) form a complex fault zone (hereinafter Düzce Fault System, DFS), up to 2.5 km wide (fig. 4.2.12) that could be part of the present-day Düzce fault damage zone [Sibson, 2003]. The northern strand of this fault system coincides with the 1999 ruptures and associated landforms, whereas branches of the RFS bound the Pleistocene bajada to the south. Most of the 1999 coseismic ruptures in the study area traversed the Pleistocene bajada (b-c-d), instead of taking place along the RFS (fig. 4.2.12). No significant ground ruptures were reported following the 1999 earthquake [Akyuz et al., 2002, Hartleb et al., 2002], or found during our own field reconnaissance, along the RFS sections. Besides the coseismic ruptures reported by Akyuz et al. [2002] along the fault g-h of figure 4.2.12, only up to 20 cm right-lateral offset ruptures were reported to us by 1999 earthquake local witnesses along 1 km of section f-g (fig. 4.2.11 and fig. 4.2.12). Although we cannot rule out shaking-related or sympathetic slip along preexisting fault traces that are embedded in and/or takes part to the damage zone, these observations may be suggestive also of some slip occurring in a wider area. This can be the reason because the coseismic slip measurements are smaller along the main northern trace of the Yenikoy, Cinarli and Beykoy subsections with respect to the Efteni subsection (fig. 4.2.6b and b-c-d-e in fig. 4.2.12).

Short/long-term tectonic landforms along the Yenikoy and Cinarli sections suggest the persistence of the 1999 rupture complexity through several seismic cycles. However, these sections have hosted a smaller cumulative deformation and express younger morphologies with respect to the RFS. This suggests that: (1) the faults bounding the embayment to the south (b-f-d in fig. 4.2.12) were the principal strands of the DFS in the past (sketches 1 and 2 in fig. 4.5.3), (2) the

Yenikoy and Cinarli subsections (b-c-d) started to be active (or to increase their activity) during or after the bajada deposition (sketches 3 and 4 in fig. 4.5.3) and now accommodate most of the Düzce fault slip.

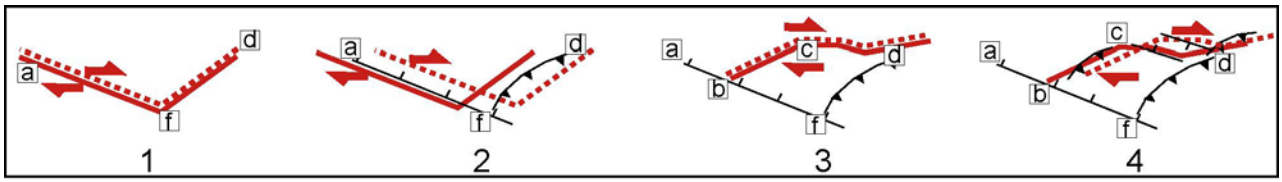

Fig 4.5.3 b) Schematic evolution of the Düzce fault system in the study area. Red arrows show relative movement of the two fault sides (dashed and continuous red lines). 1- The range front faults (a-g and f-d) start to be active (Middle/Late Miocene or Late Pliocene); 2- The geometry of the range front faults produce extensional (a-f) and compressional (f-d) local stress fields (up to Early/Middle Pleistocene ?); 3- The northern strand (b-c-d) starts to be active (Late Pleistocene?); 4- The geometry of the Yenikoy (b-c) and Cinarli (c-d) subsection produce compressional and extensional local stress fields respectively.

The northward migration of faulting, which the interpretation above implies, translates to a tendency of the fault to simplify a major geometric complexity towards a straighter trace. This is in agreement with the combination of displacement along Riedel and P-shears that leads to the formation of Y-shears, oriented parallel to the general direction of movement [Tchalenko, 1970; Woodcock and Schubert, 1994] that is presumably a mechanically more favourable setting. The presence of the intermediate faults between the 1999 ruptures and the RFS (x in fig. 4.2.12), that look older than the short/long-term landforms along the coseismic ruptures, could be suggesting that we are seeing a sequence of newer fault traces stepping out from the range front with time.

In summary, the broader geologic and geomorphic setting in the key area shows a kilometre-scale wide fault system (DFS) that ruptured during the 1999 earthquake in correspondence of the PDZs (CFT) (fig. 4.2.12). The DFS at the surface has been evolving through time forming the younger Yenikoy and Cinarli subsections (fig. 4.5.3) and contributing in the growth of the damage zone. Since there are no seismic lines available and the seismologic and the geodetic data of the study area can not resolve the complexities of the near-surface and of the far-field, is not possible to determine if parts of the RFS are directly connected to the principal fault (PSZ) at depth or not. However, even though the 1999 surface ruptures suggest that most of the strain is accommodated by

the northern part of the DFS (PSZ), the possibility that some amount of distributed permanent shear strain also develop coseismically at depth and that other structures composing the RFS, although secondarily, participate in the deformation, cannot be ruled out.

4.5.1.3. Large scale vs. small scale patterns

The patterns of 1999 ruptures and long-term deformation exhibit essentially the same en-échelon arrangement of left-stepping transtensive structures and right-stepping transpressive structures, both at meter-scale and kilometer-scale. Thus, it is noticeable that the faults arrangement is scale independent, persisting at the SDZ, at the PDZ and at the fault subsection scales (see fig. 4.2.4, fig. 4.2.6 and fig. 4.5.1). Looking at the coseismic ruptures at a meter scale it is possible to observe a reduced scale analogue model of the four rupture subsections in the study area: R-shears and T-shears at releasing bends (Efteni Lake subsection); P-shears and folds at restraining bends (Yenikoy and Beykoy) (fig. 4.5.4).

A similar analogy can be proposed between the coseismic meter-scale rupture pattern to the broader scale long-term fault system (RFS) depicted in figure 4.2.12. The a-b-f and f-d-e range front faults of the latter can be interpreted as Riedel shears and P-shears or Thrust-shears, respectively, underlined in figure 4.5.4.

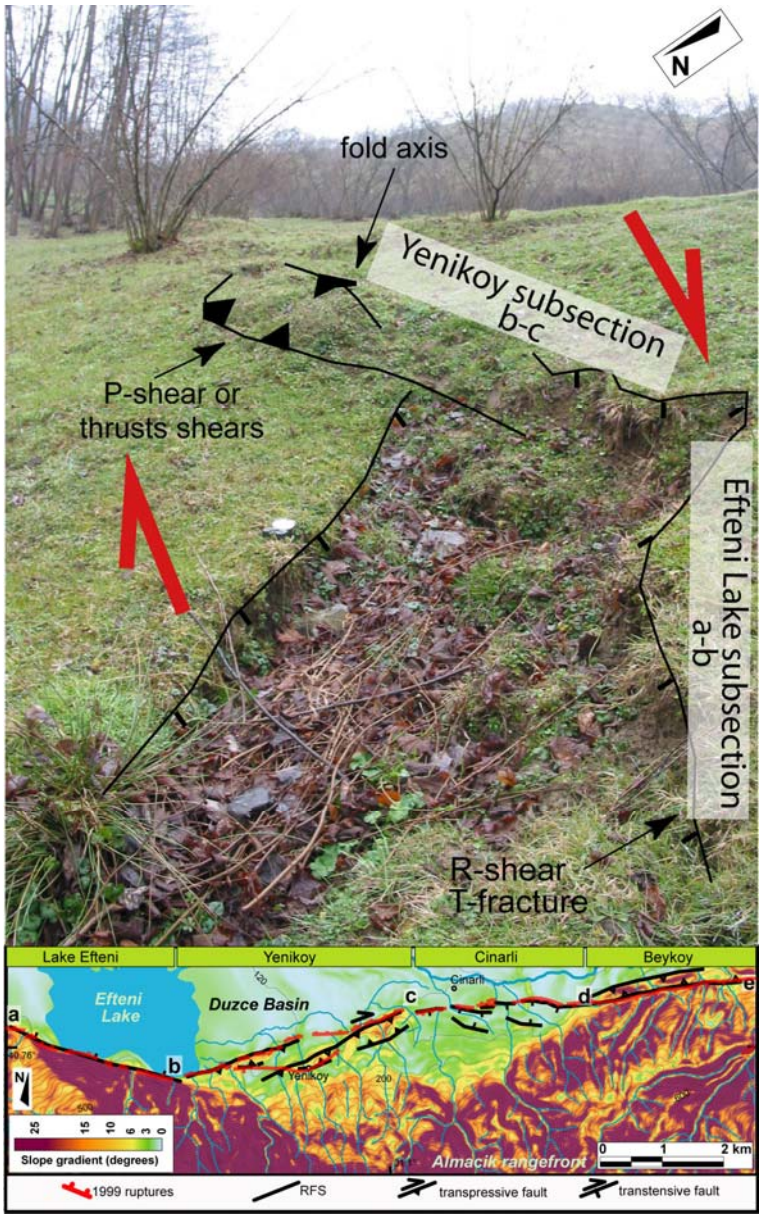

Figure 4.5.4. Detail of the 1999 surface rupture. It is noticeable that main features are scale independent analogue of both the fault pattern of two of the rupture subsections and the far-field scale fault (a-b and b-c of RFS, see Efteni Lake and Yenikoy subsections in the inset).

4.5.2. Insights from the whole Düzce fault

4.5.2.1. CFT versus RFS

Also the CFT of the whole Düzce fault is associated with a consistent pattern of landforms, indicating that the Düzce fault ruptured during repeated seismic cycles with similar location, geometry and kinematics (Plate 1a). In fact, the CFT overprinted the short/long-term tectonic morphologies, such as pressure ridges, linear valleys, escarpments and flat irons that have been

shaped on both Pleistocene-Holocene continental deposits and bedrock (see Chapter 4.3.3). However, there is a marked difference between the eastern E-W trending CFT, that exhibits more prominent landforms, and the few E-W trending portions of the western CFT, presenting weak short/long-term tectonic morphologies. As discussed in Chapter 4.5.1.2, the comparison between CFT and RFS is suggestive of a tendency of the fault to simplify a major geometric complexity (Riedel shear arrangement) towards a straighter and mature trace that is presumably a mechanically more favorable setting for the fault to rupture. This evolution is in agreement with the results of analog deformation experiments, designed to evaluate the structural patterns that develop in sedimentary strata above a deep-seated strike-slip fault [Riedel, 1929; Tchalenko, 1970; Wilcox et al., 1973; Naylor et al., 1986; see Chapter 2.1.1] (fig. 4.5.5).

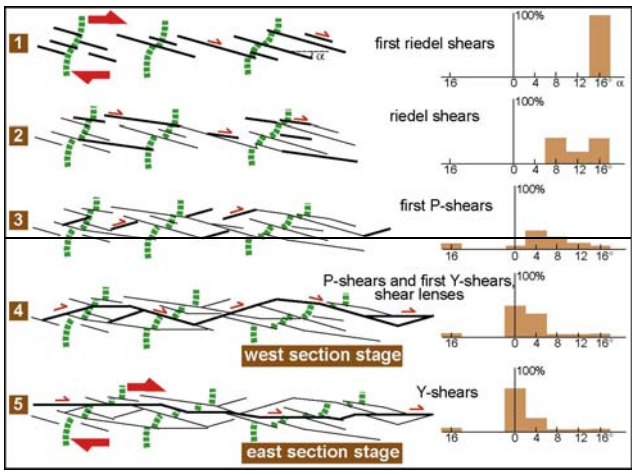

Figure 4.5.5. Sequence of structures in the Riedel experiment. Grey dashed lines mark the cumulative offset. α indicates the inclination of shear in degrees with respect to general direction of movement. Histograms show cumulative amount of displacements on shears at each stage of the deformation. (modified from Naylor et al. [1986]).

Thus, it is possible to suppose that: a) the RFS and CFT are the superficial expression of the Düzce fault at depth; b) the RFS and the CFT did not develop simultaneously but they represent different stages of evolution (*i.e.*, early and mature stages, respectively); c) on the basis of the relationships between CFT and RFS, the Düzce fault can be subdivided into two main sections the eastern and western ones approximately separated by the Cakirhaciibrahim village; d) the western section of the CFT is predominantly controlled by the RFS arrangement and contains still immature

E-W strands (incipient Y-shears, stage 4 in fig. 4.5.5); e) the eastern section is presently controlled by clear and mature E-W strands (Y-shears, stage 5 in fig. 4.5.5), accommodating most of the Düzce fault slip at the surface with the RFS completely overcome.

Given their characteristics and organization at the surface, both the RFS and CFT may correspond to the complex surface expression of a "tulip" or "palm-tree" structure due to pure strike-slip basement movement on a master fault at depth (*i.e.*, Düzce seismogenic fault). Interestingly, this geometry has been also illuminated by trapped waves studies, in fact, analysis of anomalous features from the Düzce area seismograms shows a low-velocity layer interpreted as a kilometric-broad damage-zone, 3-4 km deep [Ben-Zion et al., 2003, Peng and Ben-Zion, 2004].

4.5.2.2. The interaction between the Düzce and Karadere fault sections

An outcome of the elastic dislocation modeling (see Chapter 4.4) is that the Düzce basin can not be considered, as whole, an active pull-apart basin. In fact, the Golyaka fault-wedge area is experiencing a present-day important subsidence, whereas the north-western part of the Düzce basin is shrinking because of the Karadere fault section activity causes the north-eastward motion of the block to its north (fig. 4.4.1). These dislocation models suggest that the transtensional strain field, described by the geological and geomorphological field data along the western part of the Düzce segment, derives from the mechanical interaction between Karadere and Düzce faults. In fact, these two faults show a non-parallel overstepping zone, characterized by obliquely divergent relative fault block motions, that could represent potential location for changes in the regional stress directions and for the production of complex fault/fracture meshes similar to parallel overstepping zone [Segall and Pollard, (1980); Sibson, 1985].

Predictable geometric relationships exist between both the axis of maximum infinitesimal strain ($\cong \sigma_3$), expressed by the angle β, and the far-field transport direction expressed by the angle α and the orientations of the deformation zone boundary (see Chapter 4.3.1, fig. 4.3.7) [De Paola et al., 2005]. According to these relationships, the angle β of 50°, measured along the western section,

reveals fault block motion vectors that form an angle α of 10° from the Düzce fault boundary (fig. 4.5.6a), denoting the presence of wrench dominated transtension. The RFS could have been inherited from previous tectonics and reactivated to accommodate the oblique displacements derived from the transtensional strain field affecting the western section of the Düzce Fault, which imply accommodating the pure shear added to the simple shear (3D strain, see Chapter 2.1.2). The 3D strain appears to be slightly partitioned (see De Paola [2004] and reference therein) into adjacent different fault subsections (WNW-ESE, WSW-ENE and E-W), that accommodate differing proportions of strike-slip and dip-slip displacements. The WNW-ESE elements seem to accommodate a larger dip-slip component (fig. 4.3.6), that is also shown by the tendency of the MSR to rotate toward the PDZ (fig. 4.3.5) and by the change to a mole-track style that suppresses the push-ups (fig. 4.3.8). If this is the case, the saw-toothed CFT of the western section may be composed by a quadrimodal fault pattern (WNW-ESE and WSW-ENE subsections), as characteristic of wrench-dominated transtension, and by parallel margin component of the displacement (E-W subsections). This fault architecture appear to not have the possibility to evolve toward a simple E-W trace, such as the eastern section, implying that the complex fault pattern is a stable structural arrangement (fig. 4.5.7b). If this is the case, the compressional structures along the WSW-ENE Yenikoy subsection may be related to folding in transtensional stress field (see Chapter 2.1.2).

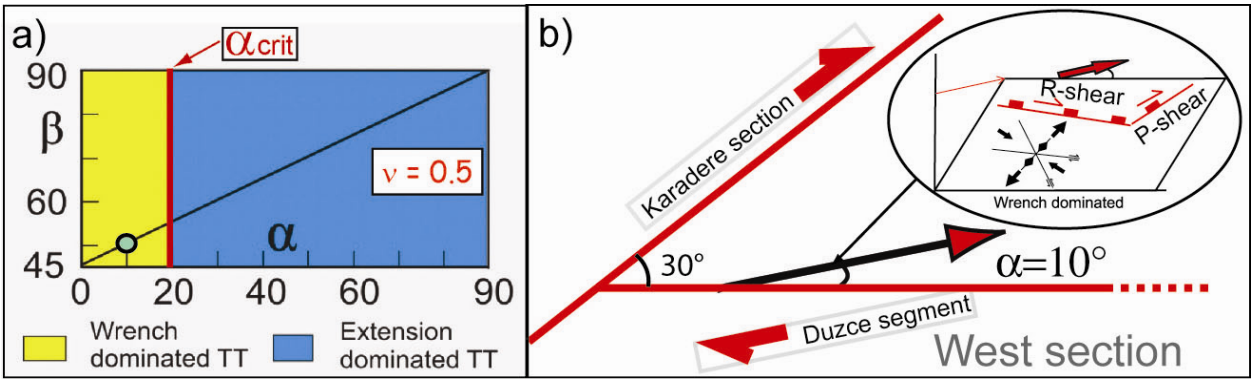

Figure 4.5.6. a) Diagram showing the relationships between the angle (β) and the angle (α) of the fault block motion vectors. Green dot refers to the west section of the CFT. (modified from De Paola et al. [2005]). b) Sketch of the geometrical relationships between the west section of the CFT and the Karadere. The west section CFT motion vector and the quadrimodal set of structures expected in wrench-dominated transtension are reported.

Interesting remarks derive from the observation that the structures along the western tip of the Düzce fault were activated (producing minor slip) during the Izmit event, three months before the November 1999 mainshock (fig. 4.5.7). The Izmit rupture could have produced strong dynamic off-fault stresses that caused extensive secondary ruptures at locations off the main fault plane. As expected, this secondary faulting occurred along the most favored extensional side, with the predictable orientations (see Chapter 2.1.7, fig. 2.1.28). The occurrence of these ruptures could have been also facilitated by the perturbation of the stress field of the Düzce fault tip that could have experienced a stress concentration due to a previous slip along the segment (see Chapter 2.1.7, fig. 2.1.26). The large number of tensile cracks, which have been generated near the western Düzce fault tip during the Izmit event, present orientations at ~25° from the fault ([Komut, 2005]; fig. 4.5.7). Their kinematics are consistent with the predicted extensional quadrant stress field of the Düzce fault tip and the small angle, that the tensile cracks orientations formed with respect to the Düzce Fault, indicates transtensional strain field, as predicted by the linear elastic fracture mechanics theory (see Chapter 2.1.7).

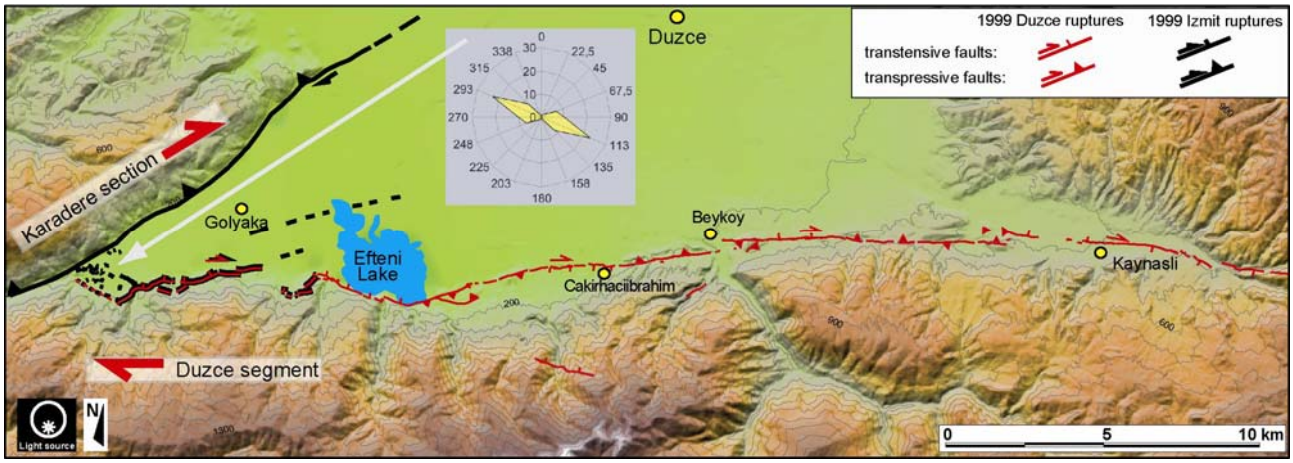

Figure 4.5.7. Traces of the 1999 Düzce (red) and Izmit (black) surface ruptures. Orientation of the tensile cracks [Komut, 2005] are reported.

4.5.3. Comparing data from surface and depth

To understand if the surface observations may shed light on the structure at depth, the surface data discussed above were compared with the Bouin et al. [2004] model of the 1999 coseismic slip distribution at depth (fig. 4.5.8). This model is overall in agreement to other source models proposed by other Authors [*e.g.*, Bürgmann et al., 2002; Utkucu et al., 2003; Çakir et al., 2003; Birgören et al., 2004]). Interestingly, this comparison shows that the projection at depth of the boundary between the western and the eastern Düzce fault sections, defined at the surface, coincides with an abrupt decrease of the horizontal slip distribution at depth (fig. 4.5.8a). In fact, this boundary separates a portion of fault plane containing a single asperity formed by two main patches of ca.6 m maximum slip to the east, and a portion with low slip, generally not exceeding 2 m, to the west. However, the slip boundary (*i.e.*, discontinuity) at depth coincide at the surface: only with a change in the arrangement of the structural pattern and not with a relevant change of strike-slip. The projection at depth of the boundary between the western and the eastern Düzce fault sections coincides also with differences of the dip-slip distribution at depth (fig. 4.5.8b): it separates a portion of fault plane showing negligible slip to the east, and a portion with up-to-2 m slip, to the west, mimicking the surface dip-slip distribution.

A possible explanation for the difference between the two Düzce fault sections both at depth and surface can be found in the interaction Karadere-Düzce faults. As discussed in the previous chapter, this interaction seems to result in the generation of a transtensional strain field across the Düzce fault. This, on the one side could be responsible for the architecture of the western Düzce section at the surface (saw-tooth style, stage 4 in fig. 4.5.5) and, on the other, it could be responsible for the lack of asperities at depth.

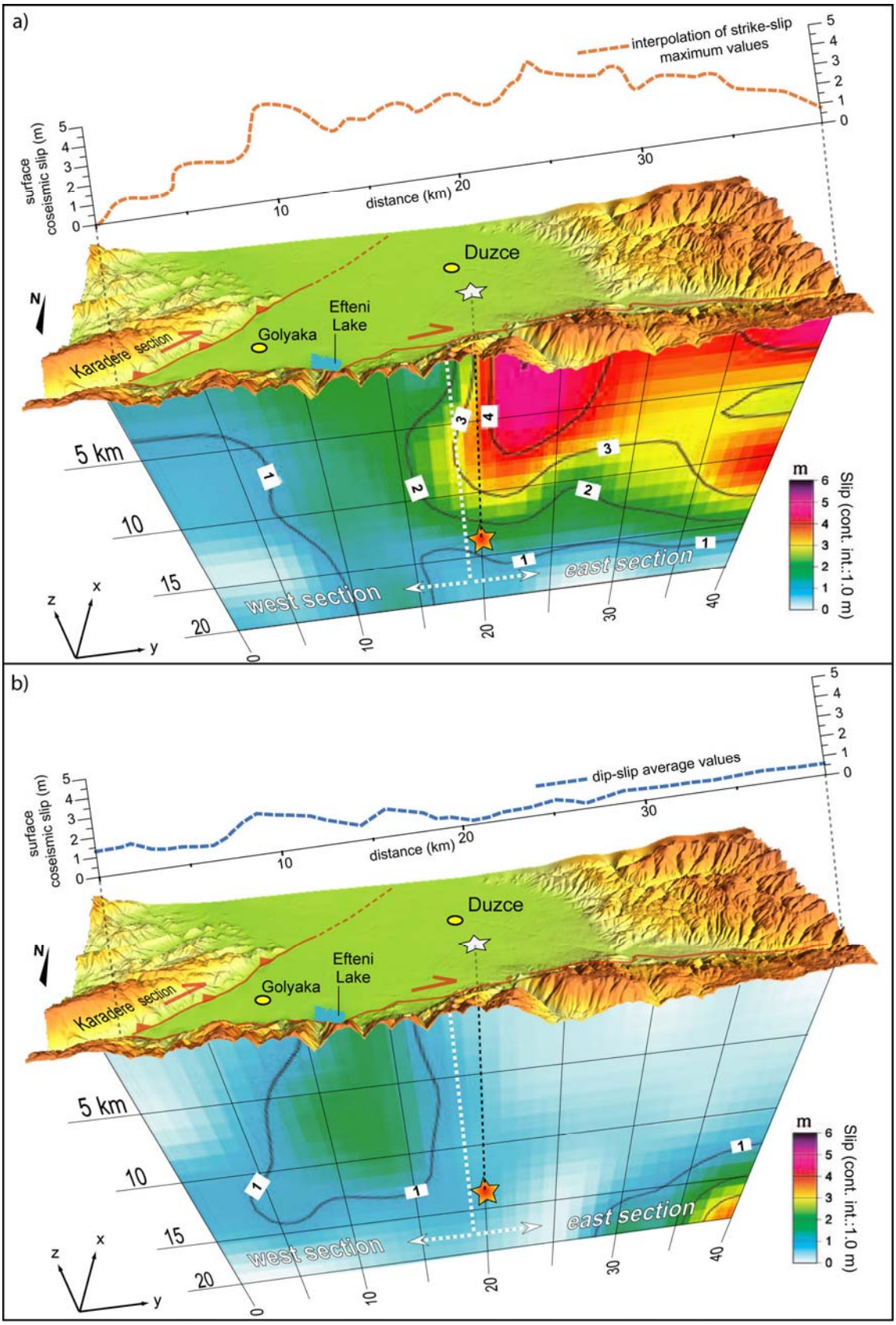

Figure 4.5.8. Block diagram showing the coseismic strike-slip distribution at depth of the Düzce rupture (at scale) for a comparison with the structures, morphology and coseismic strike and dip-slip distribution at the surface. Dashed white line indicates the boundary between the two Düzce fault sections. Hypocentre and epicentre of the mainshock are reported. [modified from Delouis et al., http://www.seismo.ethz.ch/srcmod].

Notably, the 4.5 m maximum strike-slip observed in the western Düzce fault section at the surface clearly contrast to the 2 m maximum strike-slip at depth. An open question remains how to explain this discrepancy between the horizontal coseismic slips in the western section: large at the surface and the low at depth. Because the regional tectonic loading at the scale of the fault should be considered constant, the missing coseismic slip at depth should be accommodated in a different way. Possibilities are: 1) dynamical properties of the rupture; 2) microseismicity; 3) aseismic release, with minor stress storage during the interseismic phase; 4) strain transfer to the eastern asperity as velocity-strengthening frictional afterslip [Hearn et al., 2002] during the postseismic phase; 5) partitioning of the slip between the Karadere and western part of the Düzce fault; 6) concurrence of the above hypotheses.

The transtension in the western part of the Düzce fault originating from the Karadere-Düzce mechanical interaction may play a role also in the rupture propagation. According to studies on dynamics of the rupture, the dominant factor affecting rupture propagation beyond fault discontinuities (*i.e.*, step-over, bend, double bend, fault junction) is normal stress rather than shear stress [Kase and Kuge, 2001, and references therein]. When fluid pressure differentials are not able to act as barrier [Sibson, 1985], a lower normal stress induced by local transtensional stress along the discontinuity favors the rupture propagation, but lowers its velocity and delays its triggering on the contiguous fault segment [Harris and Day, 1993 and 1999]. Under this light, the Karadere-Düzce release fault junction could also have driven the delayed propagation of the August 17, 1999 Izmit rupture on the Düzce fault, which nucleated on the asperity of its eastern section three months later, on November 12, 1999.